Journal Pre-proof

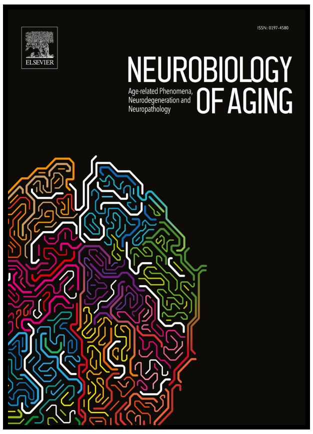

Sex and APOE4-specific links between cardiometabolic risk factors and white matter alterations in individuals with a family history of Alzheimer's disease

Stefanie A. Tremblay, R. Nathan Spreng, Alfie Wearn, Zaki Alasmar, Amir Pirhadi, Christine L. Tardif, Mallar M. Chakravarty, Sylvia Villeneuve, Ilana R. Leppert, Felix Carbonell, Yasser Iturria Medina, Christopher J. Steele, Claudine J. Gauthier

PII: S0197-4580(25)00042-9

DOI: https://doi.org/10.1016/j.neurobiolaging.2025.03.003

Reference: NBA11803

To appear in: *Neurobiology of Aging*

Received date: 25 September 2024
Revised date: 11 February 2025
Accepted date: 2 March 2025

Please cite this article as: Stefanie A. Tremblay, R. Nathan Spreng, Alfie Wearn, Zaki Alasmar, Amir Pirhadi, Christine L. Tardif, Mallar M. Chakravarty, Sylvia Villeneuve, Ilana R. Leppert, Felix Carbonell, Yasser Iturria Medina, Christopher J. Steele and Claudine J. Gauthier, Sex and APOE4-specific links between cardiometabolic risk factors and white matter alterations in individuals with a family history of Alzheimer's disease, *Neurobiology of Aging,* (2025) doi:https://doi.org/10.1016/j.neurobiolaging.2025.03.003

Title

Sex and APOE4-specific links between cardiometabolic risk factors and white matter alterations in individuals with a family history of Alzheimer's disease

Authors

Stefanie A. Tremblay[a,b,c], R. Nathan Spreng[d,e,f,k], Alfie Wearn[d], Zaki Alasmar[c,g], Amir Pirhadi[h,i], Christine L. Tardif [d,f,j], Mallar M. Chakravarty[e,j,k], Sylvia Villeneuve[e,f,k], Ilana R. Leppert[d,f], Felix Carbonell [l], Yasser Iturria Medina[d,f,m], Christopher J. Steele [c,g,n], Claudine J. Gauthier[a,b,c]

For the PREVENT-AD Research Group*

*Data used in preparation of this article were obtained from the PRe-symptomatic EValuation of Experimental or Novel Treatments for Alzheimer's Disease (PREVENT-AD) program (https://douglas.research.mcgill.ca/stop-ad-centre), data release 7.0. A complete listing of PREVENT-AD Research Group can be found in the PREVENT-AD database: https://preventad.loris.ca/acknowledgements/acknowledgements.php?date=[2024-08-07]

Affiliations

a. Physics department, Concordia University, 7141 Rue Sherbrooke W, Montréal, QC, H4B 1R6, Canada
b. Montreal Heart Institute, 5000 Rue Bélanger, Montréal, QC, H1T 1C8, Canada
c. School of Health, Concordia University, 7200 Rue Sherbrooke W, Montréal, QC, H4B 1R6, Canada

d. Department of Neurology and Neurosurgery, Montreal Neurological Institute, McGill University, 3801 University Street, Montreal, Quebec, H3A 2B4, Canada

e. Department of Psychiatry, McGill University, 845 Rue Sherbrooke W, Montréal, QC, H3A 0G4, Canada

f. McConnell Brain Imaging Centre, Montreal Neurological Institute, 845 Rue Sherbrooke W, Montréal, QC, H3A 0G4, Canada

g. Psychology department, Concordia University, 7141 Rue Sherbrooke W, Montréal, QC, H4B 1R6, Canada

h. Electrical Engineering department, Concordia University, 1455 De Maisonneuve Blvd. W. Montreal, QC, H3G 1M8, Canada

i. ViTAA Medical Solutions, 400 Rue Montfort, Montréal, QC, H3C 4J9, Canada

j. Department of Biomedical Engineering, McGill University, 845 Rue Sherbrooke W, Montréal, QC, H3A 0G4, Canada

k. StoP-AD Centre, Douglas Mental Health Institute Research Centre, 6875 Blvd. LaSalle, Verdun, QC, H4H 1R3, Canada

l. Biospective Inc., 1255 Peel, Montreal, QC, H3B 2T9, Canada

m. Ludmer Center for NeuroInformatics and Mental Health, 1010 rue Sherbrooke W, Montreal, Canada

n. Max Planck Institute for Human Cognitive and Brain Sciences, Stephanstraße 1a, 04103 Leipzig, Germany

Correspondence

Stefanie A. Tremblay (stefanieatremblay@gmail.com) or

Claudine J. Gauthier (claudine.gauthier@concordia.ca)

ABSTRACT

Early detection of pathological changes in Alzheimer's disease (AD) has garnered significant attention in the last few decades as interventions aiming to prevent progression will likely be most effective when initiated early. White matter (WM) alterations are among the earliest changes in AD, yet limited work has comprehensively characterized the effects of AD risk factors on WM. In older adults with a family history of AD, we investigated the sex-specific and APOE genotype-related relationships between WM microstructure and risk factors. Multiple MRI-derived metrics were integrated using a multivariate approach based on the Mahalanobis distance (D2). To uncover the specific biological underpinnings of these WM alterations, we then extracted the contribution of each MRI feature to D2 in significant clusters. Lastly, the links between WM D2 and cognition were explored. WM D2 in several regions was associated with high systolic blood pressure, BMI, and glycated hemoglobin, and low cholesterol, in both males and females. APOE4+ displayed a distinct risk pattern, with LDL-cholesterol having a detrimental effect only in carriers, and this pattern was linked to immediate memory performance. Myelination was the main mechanism underlying WM alterations. Our findings reveal that combined exposure to multiple cardiometabolic risk factors negatively impacts microstructural health, which may subsequently affect cognition. Notably, APOE4 carriers exhibited a different risk pattern, especially in the role of LDL, suggesting distinct underlying mechanisms in this group.

Keywords

White matter, cardiometabolic risk factors, LDL-cholesterol, sex differences, familial history, APOE4, myelin

Abbreviations

AD - Alzheimer's disease

APOE - Apolipoprotein E gene

BMI - Body mass index

BSR - Bootstrap ratio

CSD - Constrained spherical deconvolution

D2 - Mahalanobis distance

DTI - Diffusion tensor imaging

DWI - Diffusion-weighted imaging

FA - Fractional anisotropy

FOD - Fibre orientation distribution

GM - Grey matter

HbA1c - Glycated haemoglobin

HDL - High-density lipoprotein

LDL - Low-density lipoproteins

NODDI - Neurite orientation dispersion and density imaging

PLS - Partial least squares analysis

RBANS - Repeatable Battery for the Assessment of Neuropsychological Status

SBP - Systolic blood pressure

WM - White matter

1. Introduction

Recent findings highlight widespread white matter (WM) alterations as a key mechanism in Alzheimer's disease (AD) development and progression (Agosta et al., 2011; Araque Caballero et al., 2018; Bartzokis et al., 2003; Bartzokis, 2004a; Tian et al., 2023; Wearn et al., 2024; Yin et al., 2015). In fact, changes in WM microstructure were found to precede macrostructural atrophy and symptom onset in AD patients (Agosta et al., 2011; Araque Caballero et al., 2018; Dean et al., 2017; Desai et al., 2009; Maier-Hein et al., 2015; Nasrabady et al., 2018), which suggests myelin breakdown is an important contributor to the pathophysiology of AD (Bartzokis, 2011; Parrilla et al., 2024). The particular vulnerability of oligodendrocytes to various insults (e.g., toxins, oxidative damage) is hypothesized to result in myelin and axonal degeneration over time, precipitating other pathological changes seen in AD such as increased iron (Bartzokis, 2004a, 2011). Alterations in WM microstructure have thus been suggested as early biomarkers for AD (Adluru et al., 2014; Bartzokis, 2004a; Maier-Hein et al., 2015). Recent studies have even suggested that pro-myelinating treatments may rescue functional deficits in AD (Chen et al., 2021, 2022; Parrilla et al., 2024).

Despite WM microstructure being affected early, WM measures are not frequently included in the study of prodromal AD, as more attention has been given to grey matter (GM) abnormalities, such as loss of cortical and hippocampal GM volume (Barnes et al., 2009; W.-Y. Wang et al., 2015). Characterizing WM microstructural alterations in individuals at high risk of developing AD is thus crucial in understanding this early stage.

WM health declines during normal aging, following a trajectory often described as an inverted U-shape that peaks in middle age (Arshad et al., 2016; Bartzokis, 2004b; Kiely et al., 2022; Yeatman et al., 2014). Given the role of myelin in increasing transmission speed, its deterioration with age is closely associated with declines in cognitive function (Bartzokis, 2004b; Gong et al., 2023). Notably, age is the most important risk factor for AD, and its prevalence is known to differ significantly between sexes. While evidence is somewhat inconsistent, several studies report sex differences in myelin content and its trajectory across the lifespan (Arshad et al., 2016; Bartzokis, 2004b; Toschi et al., 2020). Furthermore, many factors influencing the trajectories of WM development and degeneration are known risk factors for AD.

A family history of AD and the E4 genotype of the apolipoprotein E (APOE) gene increase the likelihood of developing AD, with a higher risk in females (Altmann et al., 2014; Breitner et al., 1999; Farrer et al., 1997; Huang et al., 2004; Subramaniapillai et al., 2021). The APOE genotype impacts the brain's WM microstructure, likely due to its role in the transport of cholesterol, one of the main constituents of myelin (Bartzokis, 2004a). APOE4 carriers display lower myelin content and altered developmental trajectories compared to non-carriers (Dean et al., 2014; Remer et al., 2020; Triebswetter et al., 2022). Additionally, modifiable risk factors such as physical inactivity, smoking, alcohol consumption, hypertension, diabetes, obesity, and low education also contribute to AD risk (Livingston et al., 2024). Understanding how these factors impact brain health may inform future interventions.

These modifiable risk factors exhibit complex relationships with WM. For instance, obesity and hypercholesterolemia, known risks for cardiovascular disease and AD (Alfaro et al., 2018; Lamar et al., 2020; Shobab et al., 2005), show mixed associations with WM integrity and cognition (Alfaro et al., 2018; Birdsill et al., 2017; Burzynska et al., 2023; Lamar et al., 2020; Warstadt et al., 2014). For instance, while most studies report lower myelin content (Burzynska et al., 2023; Kullmann et al., 2016; Mole et al., 2020) and diffusion tensor imaging (DTI) indices of WM integrity (Kullmann et al., 2015) in obese individuals, a study by Birdsill et al. (2017) has found a positive relationship between obesity and fractional anisotropy (FA). These inconsistencies may stem from the limited specificity of DTI measures, as reductions in FA, often interpreted as a measure of WM integrity, can be due to axonal loss, but also to increased fiber orientation dispersion (Riffert et al., 2014). Advanced diffusion models such as NODDI (Dell'Acqua & Tournier, 2019; Zhang et al., 2012) and myelin-sensitive techniques such as magnetization transfer imaging are thus needed to fully capture WM microstructural properties (Campbell et al., 2018; Helms, Dathe, Kallenberg, et al., 2008).

The multifaceted interplay between risk factors and WM health may also introduce complexity, leading to seemingly inconsistent results as some factors synergistically influence outcomes while others counteract each other (Alfaro et al., 2018; Foley et al., 2014; Mole et al., 2020; R. Wang et al., 2015; Williams et al., 2019). Importantly, genetic risk (i.e., APOE4) seems to exacerbate the impact of modifiable risk factors on WM (Foley et al., 2014; Mole et al., 2020; R. Wang et al., 2015; Williams et al., 2019). Together, this evidence suggests that the combined effects of multiple risk factors contribute to alterations in WM microstructure. Therefore, integrative approaches, along with advanced WM imaging models, are needed to comprehensively assess the effects of AD risk factors on WM microstructure.

Multi-modal imaging and multivariate frameworks that combine several parameters are promising avenues to harness the complementarity of different neuroimaging-derived metrics (Tardif et al., 2016). One such approach, the Mahalanobis distance (D2) (Mahalanobis, 1936), provides an individual-level measure of deviation relative to a reference group, where voxels with greater D2 values in an individual represent WM areas that differ to a larger extent from the reference group. D2 is a squared distance measure between a point (i.e., measurements in an individual) and a distribution (i.e., reference data) in a multi-dimensional space, integrating several MRI metrics while accounting for covariance between metrics (Fig 1). We previously demonstrated that this method yields an integrative index that meaningfully reflects underlying microstructure in WM in line with known neuroanatomy (Tremblay et al., 2024), and that relates to cognitive and motor function in normal participants (Alasmar et al., 2024).

In this study, we computed voxel-wise deviations in WM microstructure (WM D2) in a cohort of older adults with a family history of AD. We characterized the relationships between known risk factors for AD (education, BMI, blood pressure, cholesterol, and HbA1c) and WM D2 in each sex. The effect of APOE4 genotype on the relationships between risk factors and WM microstructure was also assessed and links with cognition were explored in regions of interest.

2. Methods

2.1 Participants

The study population was taken from the PResymptomatic EValuation of Experimental or Novel Treatments for Alzheimer's Disease (PREVENT-AD) cohort which is composed of older adults (≥ 55 years old) with a familial history of Alzheimer's disease (parental or multiple-sibling) (Tremblay-Mercier et al., 2021). Most participants had a maternal history of AD-like dementia (72.4%), 37.3% had a paternal history, and 9.7% a sibling history. While the majority of participants had a single first-degree relative with AD (82.1%), some had 2 first-degree relatives with AD (16.4%) and a few had 3 (1.5%). Several participants (71.4%) also had other family members, who were not first-degree relatives, affected by AD. The participants, who were followed longitudinally starting in 2011 (some participants are still currently being followed), were all cognitively unimpaired (MoCA > 25, or considered normal after an exhaustive neuropsychological evaluation if ≤ 25, and CDR = 0) at the time of recruitment. Participants gave informed written consent before participating in the study. The procedures of the PREVENT-AD study were approved by the McGill institutional review board and/or Douglas Mental Health University Institute Research Ethics Board. The study was performed in accordance with the ethical standards of the 1964 Declaration of Helsinki.

In this study, we used the 'stage 2' MRI data acquired in 2019-2020 (data release 6.0) with a novel imaging protocol that includes multi-shell diffusion-weighted imaging (DWI) and multi-parametric mapping (MPM). Participants who had all DWI and MPM data were included in this cross-sectional study (N= 134). Of those, 97 were female (age = 67.7 ± 4.8 years, education years = 15.3 ± 3.5) and 37 were male (age = 68.6 ± 6.5, education years = 15.7 ± 3.3). Previous time points were not used in this study since these advanced imaging protocols were not acquired in 'stage 1' (Tremblay-Mercier et al., 2021).

Table 1. Demographics data for each sex and for the sex-balanced reference group that was used for D2 calculation (mean ± standard deviation). Missing data, if any, is indicated. Significant differences between sexes are denoted by an asterisk.

	Females	Missing	Males	Missing	Reference
N	97		37		74
Age (yrs)	67.7 ± 4.8		68.6 ± 6.5		68.1 ± 5.9
Education (yrs)	15.3 ± 3.5		15.7 ± 3.3		15.5 ± 3.2

APOE4 status	35 (36.1%)	18 (48.6%)	33 (44.6%)
SBP (mmHg)	124.0 ± 13.9	127.4 ± 11.7	124.2 ± 12.3
BMI (kg/m^2)	26.9 ± 4.9	27.3 ± 4.1	27.2 ± 4.8
Total cholesterol (mmol/L)	5.52 ± 0.88* N = 1	4.80 ± 0.90*	5.19 ± 0.90
HDL (mmol/L)	1.66 ± 0.44* N = 1	1.35 ± 0.33*	1.52 ±0.44
LDL (mmol/L)	3.09 ± 0.79* N = 1	2.71 ± 0.88* N = 1	2.92 ± 0.83
HbA1c (decimal percentage)	5.42 ± 0.30	5.42 ± 0.44	5.43 ± 0.36
Hypertension treatment	22†	10	14
Dyslipidemia treatment	15	12	19
Diabetes treatment	1	4	4
MoCA	28.35 ± 1.38	27.78 ± 1.83	28.0 ± 1.59
RBANS - Immediate memory	106.5 ± 13.1	102.1 ± 12.8	105.0 ± 13.1
RBANS - Delayed memory	104.9 ± 11.4	103.6 ± 9.9	105.6 ± 9.6
RBANS - Total	101.1 ± 11.1	101.9 ± 11.7	102.6 ± 10.7

SBP - systolic blood pressure, BMI - body mass index, HDL - high-density lipoprotein, LDL - low-density lipoprotein, HbA1c - glycated haemoglobin, MoCA - Montreal cognitive assessment, RBANS - Repeatable Battery for the Assessment of Neuropsychological Status.

*Normal ranges: SBP: < 120 mmHg, BMI: 18.5 to 24.9, total cholesterol: < 5.17 mmol/L, HDL: ≥ 1.55 mmol/L, LDL: < 2.6 mmol/L, HbA1c: 4.0-5.2% (Cleeman, 2001; Karakaya et al., 2014).

†Current (at the time of the MRI) and past treatments were combined.

2.2 MRI Protocol

MRI data were acquired on a 3T Siemens PrismaFit scanner at the Douglas Research Centre. The multi-shell DWI sequence was a 2D spin-echo EPI sequence (TR = 3000 ms, TE = 66 ms, phase-encoding direction = posterior-anterior (PA), resolution = 2 mm isotropic) with 100 measurements (isotropically spaced around a sphere) across 3 diffusion-weighted shells with gradient strengths of b = 300 s/mm2 (7 volumes), b = 1000 s/mm2 (29 volumes) and b = 2000 s/mm2 (64 volumes) and 9 volumes acquired without diffusion weighting (b = 0). Five non-diffusion weighted volumes (b = 0) were also acquired in the opposite phase encoding direction (AP) for distortion correction.

An MPM acquisition was performed using three 3D multi-echo gradient echo sequences (resolution = 1 mm isotropic) with different repetition times (TR) and flip angles (α) to obtain images with predominant T1- (TR = 18 ms, 6 echoes, TE = 2.16-14.81 ms, echo-spacing = 2.53 ms, α = 20°), PD- (TR = 27ms, 8 echoes, TE = 2.04-22.20 ms, echo-spacing = 2.57 ms, α = 6°), and MT-weighting (TR = 27 ms, 6 echoes, TE = 2.04-14.89 ms, echo-spacing = 2.57 ms, α = 6°). An off-resonance MT pulse (off-resonance frequency = 2.2 kHz, duration = 12.8 ms, flip angle = 540°) was applied prior to RF excitation to obtain MT-weighting (Helms, Dathe, Kallenberg, et al., 2008). The RF transmit field was acquired using a slice-selective preconditioning radiofrequency pulse with a 2D turbo-flash readout (TR = 5000 ms, TE = 1.83 ms, resolution = 4 x 4 x 16 mm) (Chung et al., 2010), which is the standard Siemens TFL B1-mapping protocol. RF receive field inhomogeneities were estimated using a pair of PD-weighted turbo-flash sequences acquired in 3D using either a body coil or a 32-channel head coil (TR = 344 ms, TE = 1.55 ms, α = 3°, resolution = 2 mm isotropic). The MPM sequence was developed and provided by the McConnell Brain Imaging Centre of The Neuro.

A T1-weighted anatomical scan was also acquired using a 3D Magnetization-Prepared Rapid Acquisition Gradient Echo (MPRAGE) sequence (TR = 2300 ms, TE = 2.96 ms, TI = 900 ms, α = 9°, resolution = 1 mm isotropic) during the same session.

2.3 Preprocessing

We computed 14 microstructural metrics from the DWI and MPM data of the 'stage 2' time point in 134 participants of the PREVENT-AD cohort. These metrics were derived from the diffusion tensor imaging (DTI) model, the fixel-based analysis framework that derives fibre density and cross-section from fibre orientation distributions (FODs) computed using multi-tissue constrained spherical deconvolution (CSD) (Jeurissen et al., 2014), and the neurite orientation dispersion and density imaging (NODDI) model (Zhang et al., 2012). MPM was used to compute quantitative maps of longitudinal relaxation rate (R1), effective transverse relaxation rate (R2*), effective proton density (PD*), and magnetization transfer saturation (MTsat) (Weiskopf et al., 2013).

2.3.1 Diffusion Tensor Imaging

Most processing steps were performed using MRtrix3 (Tournier et al., 2019). DWI data were denoised and then preprocessed using the `dwifslpreproc` Mrtrix3 function, which includes correction for motion and Eddy currents (Eddy tool in FSL 6.0.1), and correction for susceptibility-induced distortions (topup tool in FSL) using b0 volumes of opposite phase-encoding polarities (AP). Preprocessed DWI data were then upsampled to the MPRAGE T1w image resolution (1mm isotropic). Bias field correction was performed using the N4 algorithm of ANTs (3.0) within a mask computed using the brain extraction tool (`bet`) of FSL on the b = 0 preprocessed volume (Tustison et al., 2010). A brain extraction of all DWI volumes was then applied using the b = 0 mask to remove all non-brain voxels. The tensor was derived from the bias field-corrected DWI data (using `dwi2tensor`) and DTI metrics were calculated (FA, MD, AD and RD) using `tensor2metric` (Basser et al., 1994).

2.3.2 Fixel-based analysis

The fixel-based analysis (FBA) pipeline, which allows the computation of fibre density and cross-section from FODs, was followed (Tournier et al., 2019). The workflow is described in details in (Tremblay et al., 2024) and briefly summarized here. First, MPRAGE T1-w images were segmented using the `5ttgen` FSL function of Mrtrix3, which relies on the FAST algorithm (Smith et al., 2012). Response functions for WM, GM, and CSF were computed from the uncorrected DWI data and the five-tissue-type (5tt) image via the `dwi2response` function (`msmt_5tt` algorithm) (Jeurissen et al., 2014). The response functions were then averaged across participants to generate a single response function per tissue type. Multi-shell multi-tissue CSD was performed to estimate orientation distribution functions (ODFs) for each tissue type using the `dwi2fod msmt_csd` function (Jeurissen et al., 2014). Finally, bias field correction and global intensity normalization were applied to the ODFs using `mtnormalise` (Raffelt, Dhollander, et al., 2017).

2.3.3 Registration

Multi-contrast registration was used to optimize the alignment of white and gray matter, as described previously (Tremblay et al., 2024). Population templates for WM, GM and CSF were created using the `population_template` function of Mrtrix3 (with nl_update_smooth= 1.0 and nl_disp_smooth= 0.75) from the FODs of all participants (Tournier et al., 2019). Subject-to-template warps were computed with `mrregister` and applied to brain masks, WM FODs, and DTI metrics (i.e., FA, MD, AD and RD) using `mrtransform` (Raffelt et al., 2011). A template mask, including only voxels present in all participants, was derived from the intersection of all warped brain masks (`mrmath min` function). The WM volumes from the five-tissue-type images were also warped to the group template space and averaged across participants to be used as a WM mask for analyses (thresholded at a later step).

2.3.4 Computing fixel metrics

Fixel metrics were computed as described in (Tremblay et al., 2024). Briefly, a fixel mask, containing all fiber bundle elements (i.e., fixels) for each voxel, was created by segmenting the WM FOD template (Raffelt et al., 2012; Smith et al., 2013). The WM FOD of each participant was then segmented using the `fod2fixel` function, which also provided the apparent fibre density (FD) metric. The `fixelreorient` and `fixelcorrespondence` functions were then used to ensure correspondence between the participants' fixels and the fixel mask (Tournier et al., 2019). The fibre bundle cross-section (FC) metric was derived from the warps created during registration using the `warp2metric` function. FC quantifies the extent of expansion or contraction required for a fibre bundle to align with those in the fixel template. Finally, a combined metric, fibre density and cross-section (FDC), representing the overall capacity of a fibre bundle to carry information, was calculated as the product of FD and FC.

Fixel metrics were then converted into voxel-wise maps to allow for integration with other voxel-wise metrics. For the voxel aggregate of fiber density, we used the l=0 term of the WM FOD spherical harmonic expansion (i.e., 1st volume of the WM FOD, equivalent to the sum of FOD lobe integrals), which provides a voxel-wise measure of total fibre density (AFDtotal). This approach yields more reproducible estimates than summing fiber-specific FD (Calamante et al., 2015). For the voxel aggregate of fiber cross-section, we calculated the mean of FC, weighted by

FD, using the `mean` option of the `fixel2voxel` function. This metric represents the typical expansion/contraction required to align fiber bundles in a voxel to the template fixels. Finally, the voxel-wise sum of FDC, representing the total information-carrying capacity per voxel, was computed using the `fixel2voxel sum` option.

2.3.5 NODDI metrics

The python implementation of Accelerated Microstructure Imaging via Convex Optimization (AMICO) was used to fit the neurite orientation dispersion and density imaging (NODDI) model to bias field-corrected DWI data (Daducci et al., 2015; Zhang et al., 2012). Fitting was performed within the brain mask and yielded 3 parameters: the intracellular volume fraction (ICVF, also referred to as neurite density), the isotropic volume fraction (ISOVF), and the orientation dispersion index (OD). The NODDI metrics were then warped to group space using the transforms generated previously.

2.3.6 Multi-parametric mapping

Multi-echo T1-w, PD-w and MT-w images were processed using the hMRI toolbox (v 0.3.0) in Matlab (Tabelow et al., 2019; Weiskopf et al., 2013). First, all images including field maps were re-oriented using the “AutoReorient” module. This reorientation is based on rigid-body coregistration of a reference image to an MNI template. The first T1-w echo was coregistered to the avg152T1 SPM canonical template and all other images were reoriented. Quantitative R2*, R1, PD* and MTsat maps were computed from the reoriented images and field maps using the “Create hMRI maps” module with default parameters. This is achieved by computing the mean of the first 6 echoes of each scan (i.e., T1w, PDw and MTw images), resulting in three mean images (Weiskopf et al., 2013). These images are then used to compute MTsat, the apparent R1 and the signal amplitude (A) using the Ernst equation that describes FLASH signals (Helms, Dathe, & Dechent, 2008). Effective PD (PD*) is proportional to the signal amplitude and can thus be obtained by correcting for RF receive field inhomogeneities. The PD map is 'effective' because the PD measure obtained is still partly dependent on R2* since the average across multiple echoes was used and was not extrapolated to TE=0. PD* maps are scaled to standardize the mean PD in WM to the published value of 69% which ensures that PD* maps are comparable across participants (Weiskopf et al., 2013). R1 maps are calculated by correcting the apparent R1 maps for local RF transmit field inhomogeneities and imperfect RF spoiling. MTsat maps are computed from the averaged MT-w and PD-w images, and corrected for local RF transmit field. Lastly, R2* is calculated by performing a linear regression of the log signal of the 8 PD-w images (at different TEs).

Corrections for RF sensitivity bias, using measured body and head coil sensitivity maps, and for B1 transmit bias field using the TFL B1 mapping method (requires an anatomical image and a flip angle map) were also performed within the “Create hMRI maps” module. MPM maps were warped to the group space.

2.4 Computing multivariate distance metric (D2)

The MVComp toolbox was used to compute D2 from the 14 WM features (FA, AD, RD, MD, AFDtotal, meanFC, sumFDC, ICVF, ISOVF, OD, R2*, R1, PD* and MTsat) (Tremblay et al., 2024). The first step in computing D2 is to determine the reference from which the multivariate distance will be calculated. Here, because the sample is unbalanced in terms of sex, a sex-balanced reference was built from the 37 male participants and 37 randomly selected females. Demographic characteristics of the reference group, shown in Table 1, were representative of the full sample in terms of age (68.1 ± 5.9), education, cognitive status, and other risk variables. Group averages were then computed from the reference group (N = 74) for each of the 14 metrics using the `compute_average` function of MVComp. The `norm_covar_inv` function was then used to compute the covariance matrix (s) and its pseudoinverse (pinv_s) from the reference. A figure showing the correlations between MRI metrics was generated using the `correlation_fig` function which uses the covariance matrix (s) to calculate correlations (Fig 1). D2 was then computed within MVComp according to this equation:

$$D^2 = (x - m)^T C^{-1}(x - m), \qquad \text{(Equation 1)}$$

where *x* is the vector of data for one observation (e.g., one participant), *m* is the vector of averages of all observations for each independent variable (i.e., MRI metrics), and C^{-1} is the inverse of the covariance matrix. Dividing by the covariance matrix scales variables and accounts for their covariance structure. The `model_comp` function allows the computation of voxel-wise D2 between each participant and the reference average within a specified mask of analysis. Here, a WM mask generated from the average of the WM volumes of the five-tissue-type images of all participants was provided and the threshold was set at 0.99 to limit partial volume effects. The `model_comp` function yields a matrix containing the D2 data of all participants (of size: number of voxels x number of participants). The `dist_plot` function was then used to obtain a D2 map (in nifti format) for each participant. The workflow for D2 calculation is illustrated in Figure 1.

To test whether a bias was introduced in reference group participants, the D2 maps of males (which were all included in the reference) were re-computed using a leave-one-out approach. This can be done in MVComp using the `exclude_comp_from_mean_cov` option of the `model_comp` function. Analyses were then repeated using these maps, allowing for comparison.

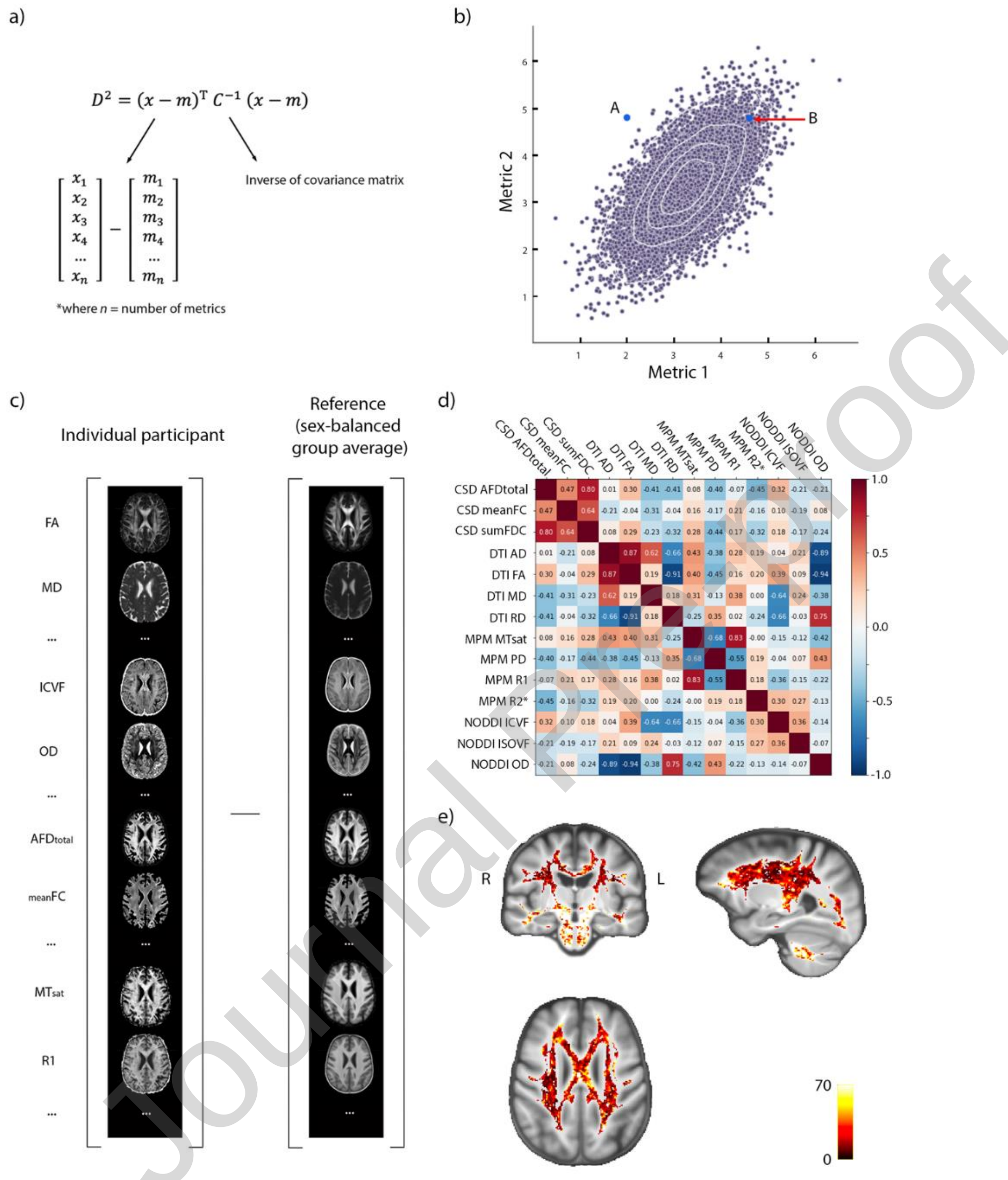

Figure 1. Methodological framework. a) Equation for computing D2. Two vectors, one containing the data of one observation (*x*) and the other containing the mean of all observations for each independent variable (*m*), are subtracted. The covariance between variables is accounted for by multiplying by the inverse of the covariance matrix (C^{-1}). b) Schematic illustration of the D2 concept in a 2-dimensional space using digitally generated correlated data. The purple dots

represent the reference distribution. The probability distance (D2) is the distance, in multivariate space, between each of the blue points (two different participants; A and B) and the distribution that takes into account the covariance structure of the data. In this example, because the two metrics are positively correlated, A will have a larger D2 value than B. c) The vectors of data are illustrated: the first contains the data of one participant (*x*) and the second contains the reference group average (sex-balanced group) for each metric (*m*). d) The correlation matrix shows relationships between MRI metrics, highlighting the importance of accounting for covariance between variables in multivariate frameworks. e) Example D2 map of a participant. The intensity indicates the amount of deviation in the WM microstructure of this participant compared to the reference, at each voxel. Note that D2 is unitless.

The effect of age on D2 was removed by fitting a linear model predicting voxel-wise D2 from age using LinearRegression in sklearn.linear_model and computing the residuals. Residualized D2 data were then normalized using yeo-johnson power transformation voxel-wise in sklearn (version 0.23.2). The residualized and normalized D2 data were used as inputs for the partial least squares (PLS) analysis between WM D2 and risk factors.

Since D2 is a measure of deviation from the reference distribution, the interpretation of D2 depends on the characteristics of the reference sample. High D2 could indicate a region of abnormality if the reference is healthy, or it could be indicative of WM microstructure that is healthier than that of the reference sample if the reference is generally unhealthy. Here, the mean risk variable values of the reference group were slightly higher than the normal healthy ranges for these variables (i.e., SBP, BMI, total cholesterol, LDL, HDL and HbA1c) (Cleeman, 2001; Karakaya et al., 2014), suggesting the latter case.

2.5 Blood samples

Blood samples were collected at every annual visit. Variables known to be associated with cardiometabolic risk were used in PLS analyses: total cholesterol, high density lipoprotein (HDL) cholesterol, low density lipoprotein (LDL) cholesterol, and glycated haemoglobin (HbA1c), a clinical index that reflects long-term glycemic control. We used the average of all measurements available in years prior to the MRI date (2011-2018) to reflect cardiometabolic risk history.

2.6 Body composition and physiological measures

Blood pressure (BP), heart rate, and body weight (in kg) were measured at every annual visit, while height (in cm) was measured at the eligibility visit. Here we used the average of all measurements available for BP and weight. BMI was calculated as: mean weight (kg) / height^2 (m). BMI and systolic BP (SBP) were used as 'risk variables' in PLS analyses.

2.7 APOE4 genotyping

Genotyping methods for this dataset have been described in (Tremblay-Mercier et al., 2021). Briefly, DNA was isolated from 200 µl whole blood using a QIASymphony apparatus and the DNABlood Mini QIA Kit (Qiagen, Valencia, CA, USA). Allelic variants of AD-related genes including APOE rs429358 and rs7412 were characterized using pyrosequencing (PyroMark24 or PyroMark96) or DNA microarray (Illumina). Participants were classified as either APOE4+ (N= 35 females; N= 17 males) if they had one or more E4 alleles or as APOE4- (N= 61 females; N= 19 males) if they had none. Participants with ε2ε4 were included in the APOE4+ group as this genotype has been previously reported to confer risk for AD pathologies that is similar to that of ε4 carriers (Goldberg et al., 2020). The low number of participants with two E4 alleles (N= 3 females; N= 1 male) did not allow the exploration of a dose-dependent effect of APOE4.

2.8 Cognitive assessment

The Repeatable Battery for the Assessment of Neuropsychological Status (RBANS) (Randolph et al., 1998), a brief test (less than 30 minutes) that measures performance in five cognitive domains, was administered to participants at every annual visit. The test yields scaled scores (i.e., age-adjusted index scores with a mean of 100 and standard deviation of 15) for immediate memory, visuospatial/constructional, attention, language and delayed memory. For this study, the RBANS scores of the evaluation conducted on the same day as the MRI session were used and analyses focused on the immediate and delayed memory subscores, the components that have been shown to be the best predictors of AD and mild cognitive impairment (Duff et al., 2010).

2.9 Statistical analyses

2.9.1 Relationships between WM microstructure and risk factors

Partial least squares (PLS) analyses were conducted between D2 in WM and risk factors of AD, separately in each sex. PLS is a multivariate statistical approach that can be used to describe spatial relationships between brain MRI data and multiple other variables, in our case risk factors (McIntosh & Lobaugh, 2004). PLS finds the weight vectors that maximize the covariance between brain data and risk variables, forming new variables called latent variables (LVs). Each WM voxel is assigned a weight, or salience, indicating how strongly it covaries with the pattern of the latent variable, which is a linear combination of the risk factors data.

PLS analyses were conducted in Matlab R2023b (Mathworks Inc.) using the PLS toolbox (McIntosh & Lobaugh, 2004). The "Regular Behav PLS" was selected as the type of analysis and risk factor data were loaded as the "behavioural data". Risk factor variables included: education (total number of years of formal education), SBP, BMI, HDL, LDL, total cholesterol, and HbA1c. One participant in each group (males and females) were excluded from these analyses due to missing cholesterol data (see Table 1). The analyses were run with 1000 permutations to determine the significance of each LV, and 1000 bootstraps to determine overall reliability of each voxel's association to each LV by calculating the standard error of each voxel's salience value. Only significant LVs ($p < 0.05$) and voxels with absolute bootstrap ratios (BSR) > 2 (equivalent to $p < 0.05$) were interpreted. ROIs were created using the `fsl-cluster` function. BSR values greater than the level of significance were used as thresholds for cluster creation to limit the spatial extent of ROIs (described in the Results section).

Similar analyses were conducted between D2 in WM and the same risk factors, this time disaggregating by APOE4 status (APOE4+ if one E4 allele or more, N= 52; APOE4- if no E4 allele, N= 80), irrespective of sex. ROIs were created following a similar process as described above.

Analyses were conducted separately in each group to assess patterns specific to each APOE4 group and to each sex. Patterns common to more than one group were then tested for statistical group differences using a 2x2 ANOVA with sex and APOE4 status as fixed factors and with the brain scores (usc) from a PLS analysis in the overall group as the dependent variable. This analysis allowed us to determine whether the pattern was expressed more strongly in one group compared to the others and to test for interaction between APOE4 and sex.

2.9.2 Relationships between deviations in WM microstructure and cognition

Correlation analyses were conducted between mean D2 in ROIs (significant clusters from PLS analyses) and the immediate and delayed memory subscores of the RBANS. Analyses were targeted to these two subscores, known to be the most affected cognitive domains in AD (Duff et al., 2010), and to significant clusters identified in the PLS analysis, to limit the number of comparisons. Correction for multiple comparisons was performed using the false discovery rate (FDR) Benjamini-Hochberg method (FDR-corrected p-value < 0.05 was considered statistically significant).

2.9.3 Determining feature importance in regions of interest

The relative contributions of each feature (i.e., MRI metric) to D2 in significant ROIs (of size > 100 voxels) were then extracted using the `return_raw` option of the `model_comp` function in MVComp. The `return_raw` option yields a matrix of size (number of voxels) x (number of metrics) x (number of participants). Contributions were then summarised by averaging distance values across voxels within the ROI and across participants and dividing by the total distance (for all features), resulting in one distance value per metric, expressed as a percentage, for each ROI. This analysis provides a measure of the importance of each metric in determining D2 in the ROI.

3. Results

3.1 Relationships between WM microstructure and risk factors in each sex

Significant patterns of covariance were found between risk factors for AD and WM D2 in both males and females. In males, only the first LV of the PLS analysis was significant ($p = 0.002$) and it explained 34.4% of total crossblock covariance (Fig 2a-b). Low SBP, low BMI, low HbA1c and high cholesterol (total chol, HDL and LDL) were associated with high D2 in several WM regions including the body of corpus callosum, superior corona radiata, superior thalamic radiation (bilaterally) and the right frontal aslant tract. In females, only the first LV was significant ($p < 0.001$) and explained 40.9% of total crossblock covariance (Fig 2c-d). Similar relationships were observed but in slightly different WM regions. D2 in the superior longitudinal fasciculus, corticospinal tract, cingulum, splenium of corpus callosum, posterior corona radiata, and arcuate fasciculus (bilaterally), as well as the right forceps major and body of corpus callosum was associated with these risk factors in females. Generally, associations were found in more frontal and parietal regions in males, while they were found in more posterior and temporal locations in females. There were also overlapping regions in both sexes, specifically in parietal regions and in WM tracts underlying the precentral gyrus. Education was the only non-significant factor in both groups. Figure 2 shows the strength and direction of the relationships between D2 and each risk factor (left panel), as well as the WM regions in which those relationships are located (right panel). Only significant voxels ($|BSR| > 2.0$) and those belonging to clusters of size > 100 voxels are shown. Clusters were formed from significant voxels. Thresholds higher than the significance limit ($|BSR| = 2.0$, equivalent to $p = 0.05$) were used to limit the spatial extent of clusters and different cluster thresholds were used in each sex to result in similarly sized clusters, so that D2 was averaged across a similar number of voxels for analyses with cognition ($|BSR| > 2.5$ in females and > 3.0 in males). Further analyses were focused on clusters of size > 100 voxels. Cluster information, including the size, maximal |BSR| and brain region, is displayed in Table 2.

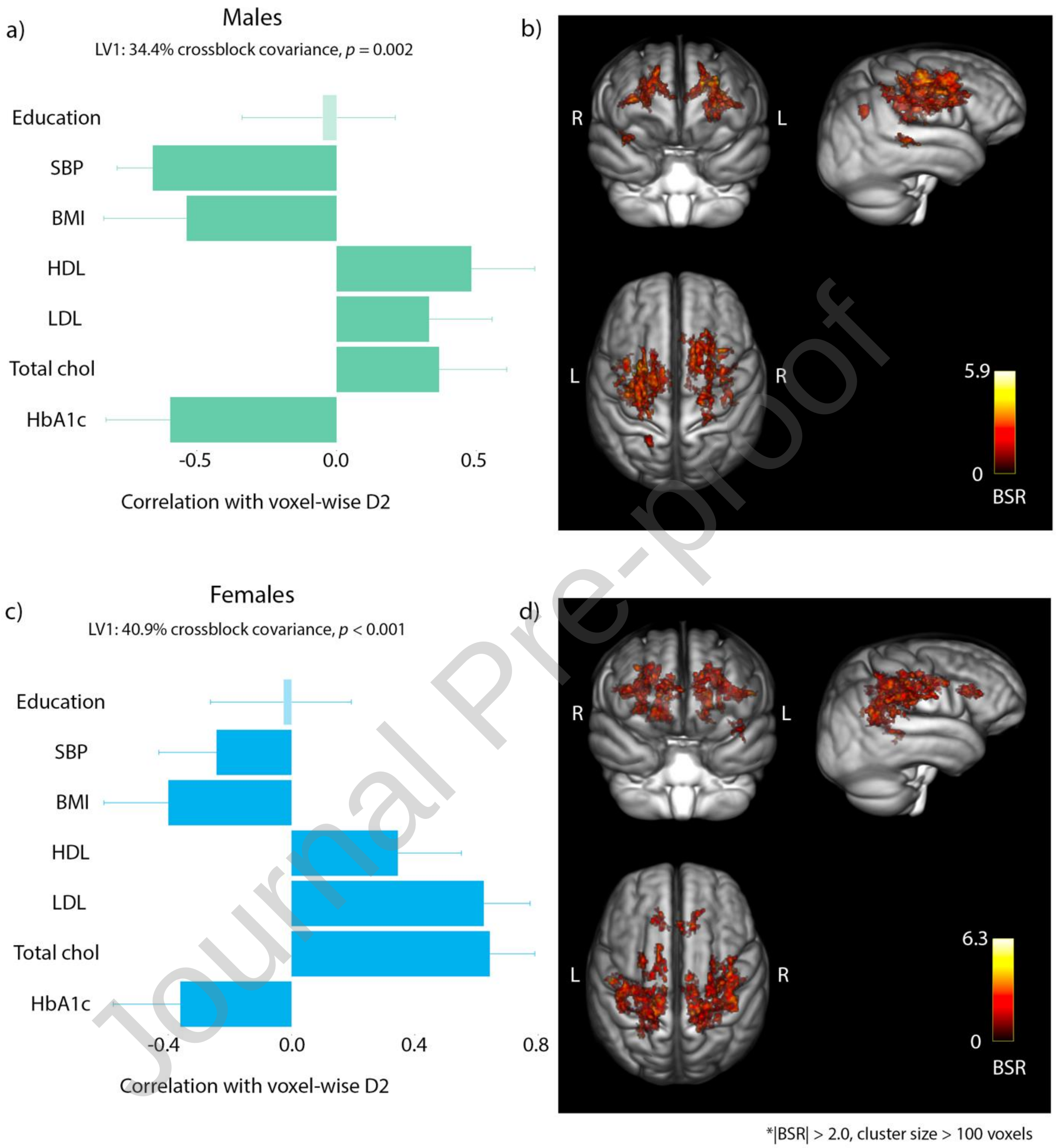

Figure 2. Relationships between D2 in WM and risk factors in each sex. Left panel (a & c): The strength and direction of the relationship that each risk factor has with D2 in the voxels shown on the brain images on the right. Error bars show 95% confidence intervals. Correlations are non-significant when confidence intervals overlap with zero (faded bar). Right panel (b & d): Colored

voxels (|BSR| > 2.0) have a positive relationship with the patterns shown in the left panel. The BSR maps are overlaid on a MPRAGE T1w group average image. Males (a-b) Several risk factors were associated with D2 across broad WM regions. Higher D2 was associated with lower SBP, BMI and HbA1c and with higher HDL, LDL and total cholesterol. Females (c-d) Similar relationships were observed in females but across different WM regions.

Table 2. Cluster information (PLS analyses in each sex). Location identified according to the JHU ICBM-DTI-81 White-Matter and XTRACT HCP Probabilistic tract atlases and cortical region closest to the WM region identified using the Harvard-Oxford cortical structural atlas.

	Size (#voxels)	**Max |BSR|**	**WM region**	**Cortical region near**
Males				
Cluster 1	346	5.63	Superior corona radiata & superior thalamic radiation L	Precentral & superior frontal gyri
Cluster 2	266	5.88	Body of corpus callosum, superior corona radiata & superior thalamic radiation L	Superior frontal & cingulate gyri, supplementary motor cortex
Cluster 3	140	4.93	Body of corpus callosum, frontal aslant tract & superior/ant corona radiata R	Superior frontal, cingulate & paracingulate gyri

Females

Cluster 1	348	5.39	Superior longitudinal fasciculus (temporal part), arcuate fasciculus R	Supramarginal, precentral & postcentral gyri, opercular cortex
Cluster 2	252	5.2	Cingulum, splenium of corpus callosum, posterior corona radiata L	Cingulate gyrus (posterior division), precuneous cortex
Cluster 3	180	5.3	Splenium of corpus callosum, forceps major & cingulum R	Cingulate Gyrus (posterior division), precuneous cortex
Cluster 4	174	5.16	Superior longitudinal fasciculus, arcuate fasciculus & corticospinal tract L	Precentral & postcentral gyri, parietal operculum cortex
Cluster 5	157	5.76	Cingulum, splenium & body of corpus callosum, posterior corona radiata R	Cingulate gyrus
Cluster 6	151	5.08	Corticospinal tract & superior longitudinal fasciculus L	Precentral & postcentral gyri
Cluster 7	107	4.66	Superior longitudinal fasciculus & corticospinal tract R	Precentral & postcentral gyri

3.2 Relationships between WM microstructure and risk factors in each APOE4 group

Different patterns of covariance were found between risk factors for AD and WM D2 in the APOE4+ and APOE4- groups. In APOE4+, LV1 ($p = 0.013$, crossblock covariance = 34.9%) and LV2 ($p = 0.048$, crossblock covariance = 22.5%) were significant. The LV1 pattern revealed that low BMI and high cholesterol (total chol, HDL and LDL) were associated with high D2 in several WM regions including the left body of corpus callosum, frontal aslant tract, superior thalamic radiation, and arcuate fasciculus (Fig 3a-b). These risk factors and their directions of association to D2 represent a subset of the pattern seen in sex-specific analyses. On the other hand, LV2 revealed a different risk pattern: low SBP, low BMI, high HDL, low LDL, and low HbA1c were associated with high D2 in the right superior longitudinal fasciculus, superior corona radiata, superior thalamic radiation, and corticospinal tract (Fig 3c-d). Generally, associations of the first LV were found in the left hemisphere and included commissural fibers such as the corpus callosum, while LV2 associations were found mostly on the right and included projection fibers such as the superior corona radiata as well as association tracts.

In APOE4-, only the first LV of the PLS analysis was significant ($p < 0.001$) and it explained 46.5% of total crossblock covariance (Fig 3e-f). The risk factors pattern was very similar to that of previous analyses (sex-disaggregated PLS analyses). Low SBP, low BMI, low HbA1c and high cholesterol (total chol, HDL and LDL) were associated with high D2 in broad WM regions including the superior longitudinal fasciculus, arcuate fasciculus, superior corona radiata, and corticospinal tract. Significant regions of the PLS analysis in APOE4- overlapped to a large extent with significant regions seen in sex analyses.

Education was non-significant in all LVs. Figure 3 shows the strength and direction of the relationships between D2 and each risk factor (left panel), as well as the WM regions in which those relationships are located (right panel). Only significant voxels ($|BSR| > 2.0$) and those belonging to clusters of size > 100 voxels are shown. Clusters were formed from significant voxels. Thresholds of $|BSR| > 2.5$ in APOE4+ and > 3.0 in APOE4- were used for clustering to result in similar size clusters across groups and further analyses were focused on clusters of size > 100 voxels. Cluster information is displayed in Table 3.

Because a general common pattern was observed in both sexes and in the APOE4- group, we performed another PLS analysis in the whole sample to test for group differences and interactions between sex and APOE4. This analysis showed a very similar pattern as that observed in these groups (Supplementary Fig 1). The ANOVA on the brain scores (i.e., usc) from this analysis revealed a significant main effect of sex ($p < 0.001$), indicating that males expressed the pattern of the LV more strongly than females (Supplementary Table 1 and Supplementary Fig 2). There were no significant APOE4 group differences and no significant sex x APOE4 interaction ($p > 0.05$) (Supplementary Table 1).

To ensure that the inclusion of male participants in the reference group had a negligible effect on the results, an analysis using maps generated with a leave-one-out approach was conducted in males. The effect should be largest in males since all male participants were included in the reference group. The results of this re-analysis closely matched the original findings, with nearly identical correlations between D2 and risk variables, as well as highly similar clusters. Detailed comparisons are provided in the Supplementary Materials (Supplementary Fig 3-4), confirming that the inclusion of participants in the reference group does not substantially impact the findings.

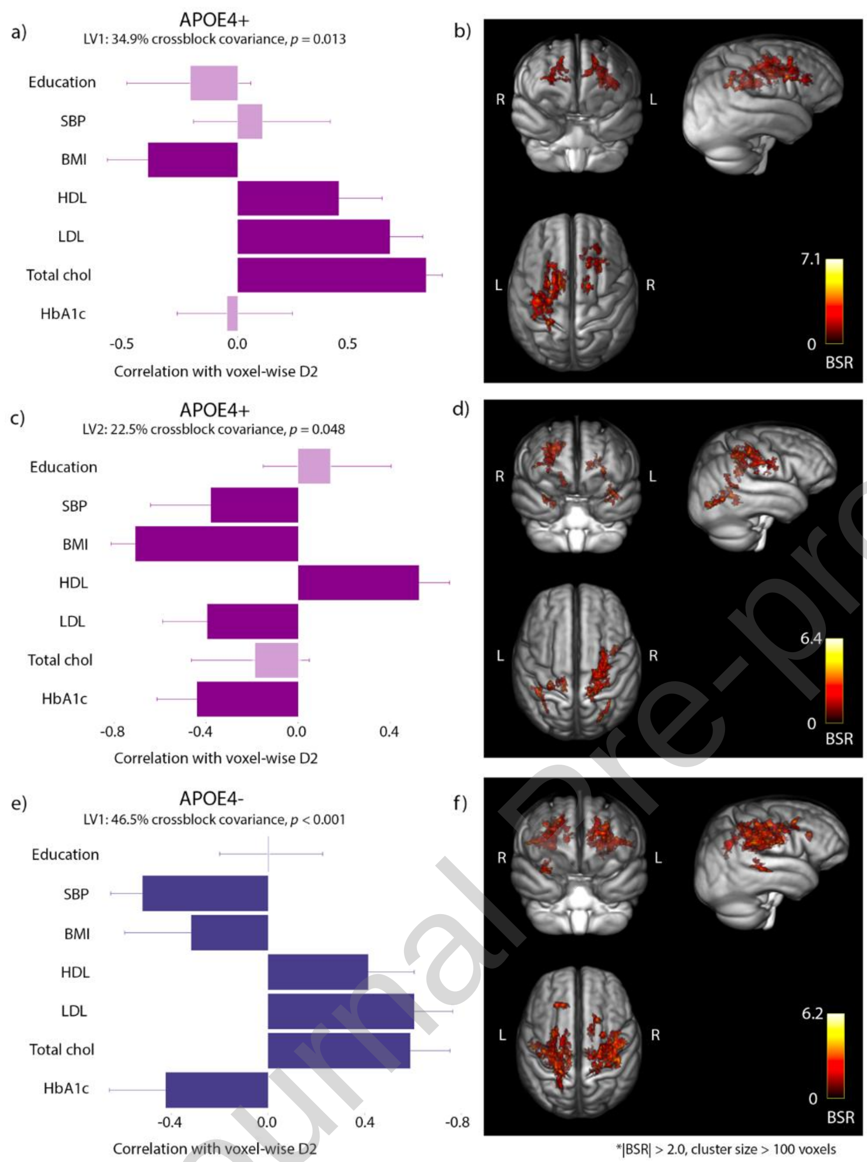

Figure 3. Relationships between D2 in WM and risk factors in each APOE4 group. Left panel: The strength and direction of the relationship that each risk factor has with D2 in the voxels shown on the brain images on the right. Error bars show 95% confidence intervals. Correlations are non-significant when confidence intervals overlap with zero (faded bar). Right panel: Colored voxels (|BSR| > 2.0) have a positive relationship with the patterns shown in the left panel. The BSR maps are overlaid on a MPRAGE T1w group average image. **APOE4+** (a-b) LV1: Higher D2 was associated with lower BMI and higher HDL, LDL and total cholesterol. (c-d) LV2: Higher D2 was

associated with low SBP, low BMI, high HDL, low LDL, and low HbA1c. **APOE4-** (e-f) Higher D2 was associated with low SBP, BMI, HbA1c and with high HDL, LDL and total cholesterol.

Table 3. Cluster information (PLS analyses in each APOE4 group). Location identified according to the JHU ICBM-DTI-81 White-Matter and XTRACT HCP Probabilistic tract atlases and cortical region closest to the WM region identified using the Harvard-Oxford cortical structural atlas.

	Size (#voxels)	**Max |BSR|**	**WM region**	**Cortical region near**
APOE4+				
LV1				
Cluster 1	499	6.27	Body of corpus callosum, frontal aslant tract & superior thalamic radiation L	Superior frontal, precentral & anterior cingulate gyri
Cluster 2	326	7.12	Superior longitudinal fasciculus & arcuate fasciculus L	Precentral & postcentral gyri, insular cortex & operculum cortex
Cluster 3	106	6.63	Superior longitudinal fasciculus L	Postcentral gyrus & superior parietal lobule
Cluster 4	100	5.31	Superior corona radiata, frontal aslant tract & superior thalamic radiation L	Superior & middle frontal gyrus

LV2				
Cluster 1	391	5.48	Superior corona radiata, superior thalamic radiation & corticospinal tract R	Precentral gyrus
Cluster 2	190	6.37	Superior longitudinal fasciculus & corticospinal tract R	Precentral & postcentral gyri
APOE4-				
Cluster 1	264	4.94	Superior longitudinal fasciculus & arcuate fasciculus R	Precentral & postcentral gyri & operculum cortex
Cluster 2	127	5.7	Superior corona radiata & corticospinal tract L	Precentral gyrus, insular cortex & operculum cortex

3.3 Determining feature importance in regions of interest

In females, features' contributions were extracted in the 7 clusters that were significant in the PLS analysis (Fig 4a). Top contributors were defined as those that contributed more than 10% to the multivariate distance D2. Exact percentage contributions of the top contributors for each cluster are indicated in figures 4-5 and in Supplementary Table 2. D2 in cluster 1 was driven mainly by MTsat, R1, and RD. In cluster 2, meanFC, R1, and MTsat contributed the most to D2. Similarly, in cluster 3, meanFC, R1, and MTsat were the top contributors. In cluster 4, R1, MTsat, and ISOVF contributed most to D2. D2 in cluster 5 was driven mainly by R1 and meanFC. In cluster 6, R1, ISOVF, meanFC, and MTsat were the metrics that contributed the most to D2. In cluster 7, D2 was mainly driven by R1, meanFC, AD, and MD. Overall, R1, meanFC, and MTsat were the most important metrics in females. The isotropic volume fraction (ISOVF) metric from NODDI was also an important contributor in 2 clusters.

In males, features' contributions were extracted in the 3 significant clusters from PLS analysis (Fig 4b). D2 in cluster 1 was driven mainly by R1 and, to a lesser extent, by AD. In cluster 2, R1, MTsat, and PD* contributed the most to D2. In cluster 3, R1 and MTsat were the top contributors. Like in females, R1 and MTsat emerged as top contributors to D2 in males. However, meanFC was not an important contributor to D2 (<10%) in any of the males' clusters.

In the APOE4+ group, there were 4 clusters from the first LV and 2 clusters from the second LV (Fig 5a-b). D2 in the first LV1 cluster was driven mainly by R1, MTsat, and PD*. In cluster 2, R1, MTsat, and meanFC were the top contributors. In cluster 3, R1, MTsat, meanFC, and ISOVF contributed most to D2. D2 in cluster 4 was driven mainly by R1 and meanFC. In cluster 1 of the second LV, R1, MTsat, and meanFC contributed most to D2. In cluster 2, MTsat, R1, and OD were the metrics that contributed most to D2.

In the APOE4- group, features' importance was extracted in the 2 significant clusters (Fig 5d). D2 in cluster 1 was driven mainly by R1, MTsat, and RD. In cluster 2, R1, MTsat, and ICVF contributed the most to D2.

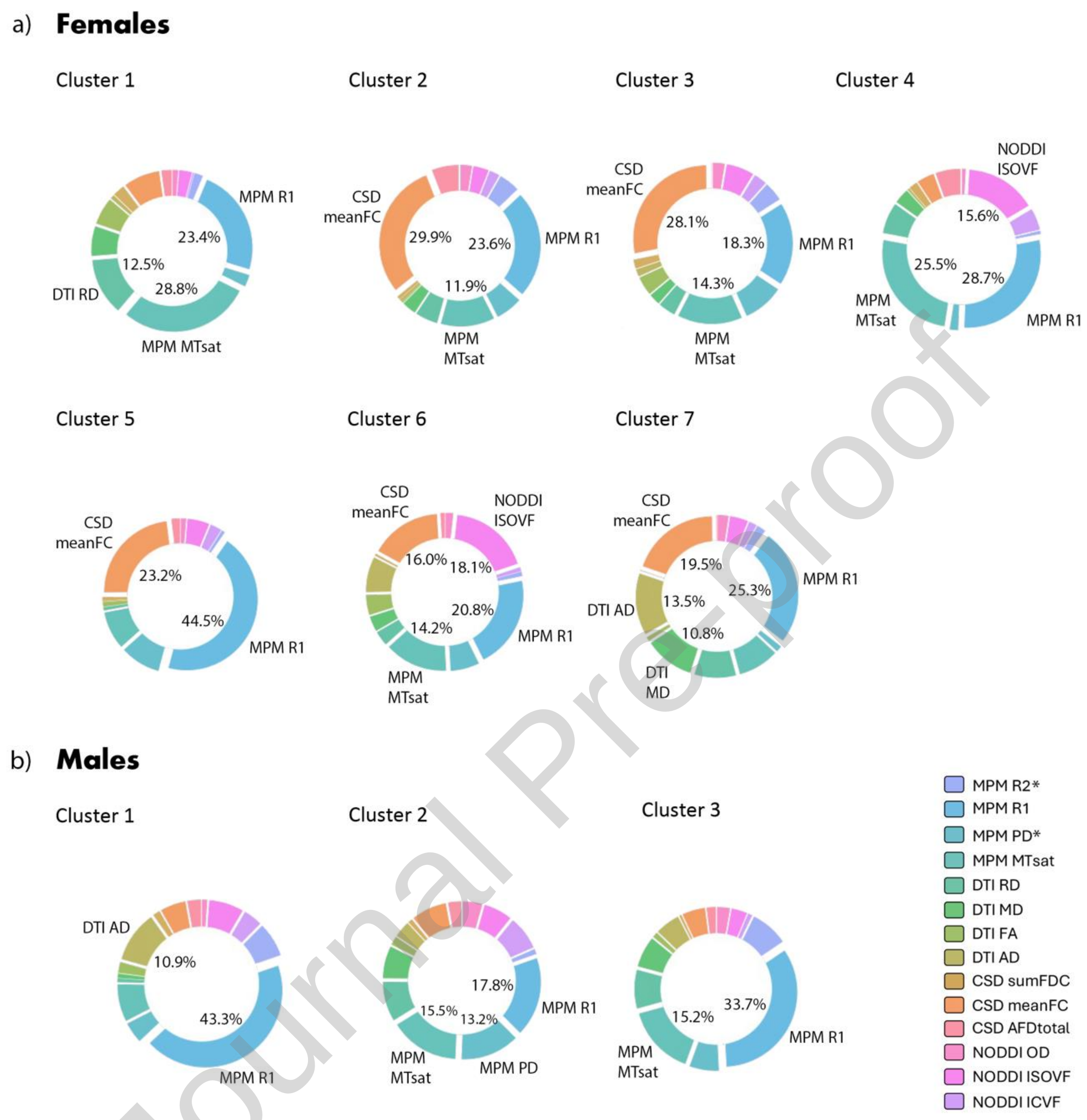

Figure 4. Features contribution to D2 in each significant cluster from PLS analyses in females (a) and males (b). For each significant cluster, the relative contribution (%) of each MRI metric is indicated by its size on the pie chart (see the legend for color of each MRI metric). The metric name and its contribution (in %) is indicated only for the most important contributors (those that account for >10%), for clarity. MPM R1 = macromolecular content (axons and myelin) (Callaghan et al., 2014); MPM MTsat = more specific to myelin content (Helms, Dathe, Kallenberg, et al.,

2008); MPM PD* = amount of water (if increased could reflect neurite atrophy); CSD meanFC = fiber bundle cross-section (Raffelt, Tournier, et al., 2017); NODDI ISOVF = amount of free water (if increased it could reflect neurite atrophy) (Zhang et al., 2012); AD = axonal integrity; RD = myelin integrity (Winklewski et al., 2018); MD = overall diffusivity (typically increased with higher water content/cell atrophy).

3.4 Relationships between deviations in WM microstructure and cognition

To understand the associations between deviations in WM microstructure and cognition, correlation analyses were performed between D2 in significant clusters from the PLS analysis disaggregated by APOE4 status (8 clusters; Table 3) and scores in the immediate and delayed memory RBANS items. D2 in the two LV2 clusters was positively associated with immediate memory. The first cluster, located in a WM region corresponding to part of the right superior corona radiata, superior thalamic radiation and corticospinal tract, had a product-moment correlation (*Pearson's*) $r = 0.313$ and a p value = 0.024 (p-fdr corrected = 0.192). Cluster 2, located in a WM region corresponding to part of the right superior longitudinal fasciculus and corticospinal tract, had a product-moment correlation $r = 0.428$, $p = 0.002$ (p-fdr corrected = 0.032) (Fig 5c). Only the correlation in cluster 2 remained significant after FDR correction. All other correlations were non-significant ($p > 0.05$).

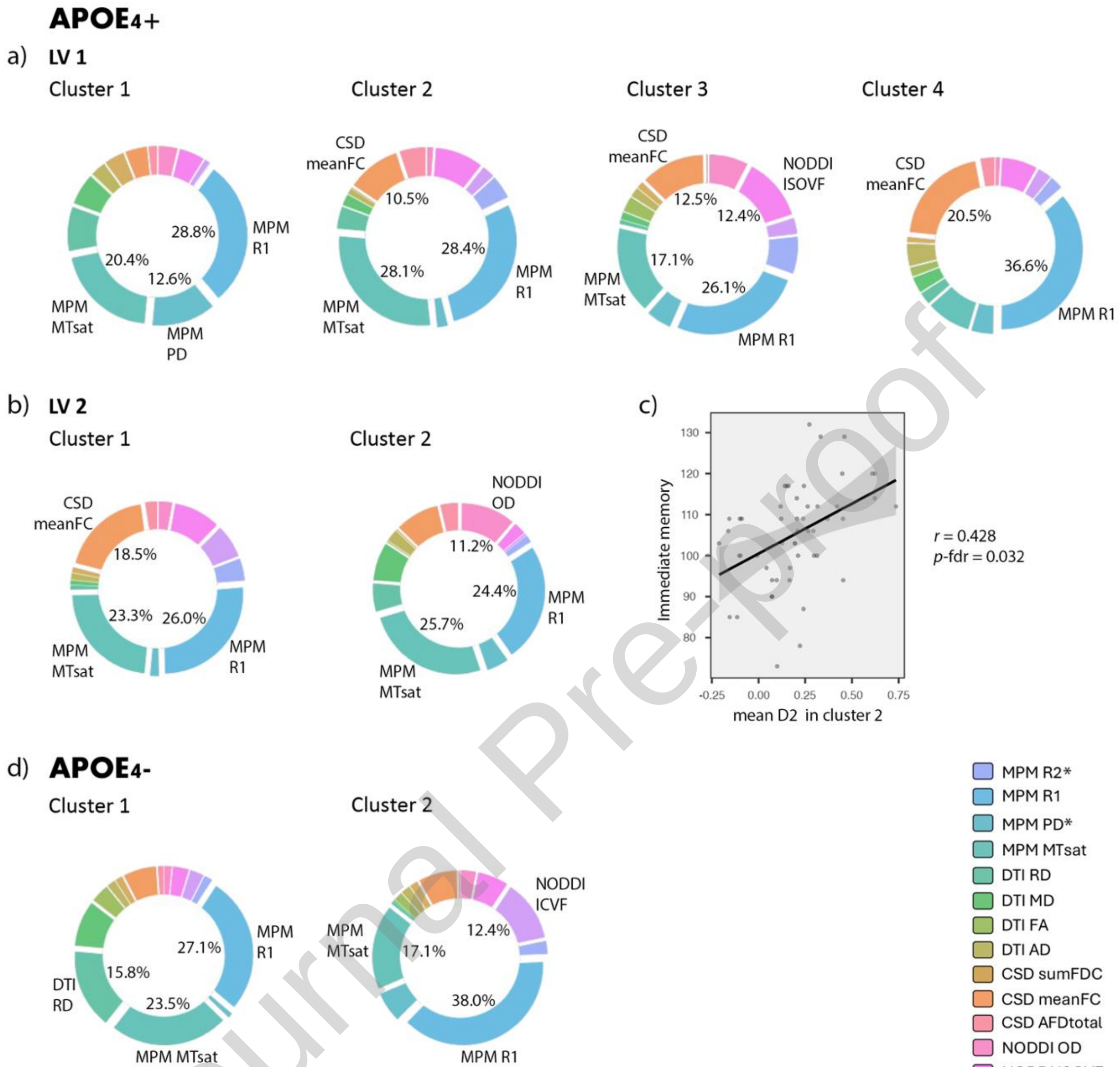

Figure 5. Features contribution to D2 in each significant cluster from PLS analyses in APOE4+ (a-b) and APOE4- (d). For each significant cluster, the relative contribution (%) of each MRI metric is indicated by its size on the pie chart (see the legend for color of each MRI metric). The metric name and its contribution (in %) is indicated only for the most important contributors (those that account for >10%), for clarity. c) Plots are shown for significant correlations between D2 and the RBANS memory items. Immediate memory was positively associated with D2 in cluster 2 of

the APOE4+ analysis (LV2). MPM R1 = macromolecular content (axons and myelin) (Callaghan et al., 2014); MPM MTsat = more specific to myelin content (Helms, Dathe, Kallenberg, et al., 2008); MPM PD* = amount of water (if increased could reflect neurite atrophy); CSD meanFC = fiber bundle cross-section (Raffelt, Tournier, et al., 2017); NODDI ISOVF = amount of free water (if increased it could reflect neurite atrophy); NODDI ICVF = neurite density; NODDI OD = orientation dispersion of fiber tracts (Zhang et al., 2012); RD = myelin integrity (Winklewski et al., 2018).

4. Discussion

In this study, we identified the presence of WM microstructural impairments linked to cardiometabolic risk factors in individuals with a family history of Alzheimer's disease (AD). These impairments were identified using a novel approach, whereby we investigated the sex-specific and APOE genotype-related relationships between WM microstructural deviations, quantified using a multivariate score derived from several MRI-derived features, and cardiometabolic risk factors. Through this double multivariate approach (using PLS analysis and the Mahalanobis distance), we were able to explore how the combined effects of multiple risk factors contribute to alterations in multiple aspects of WM microstructure. Although others have shown similar associations between AD risk factors and WM microstructural health (Burzynska et al., 2023; Kullmann et al., 2015, 2016; Maillard et al., 2012; Repple et al., 2021; Ye et al., 2024), few have assessed these relationships as comprehensively as the current study, using both advanced and more conventional MRI metrics to characterize WM properties, and investigating such a wide array of risk factors. Consistent with the extant literature on myelin trajectories and vulnerability (Arshad et al., 2016; Bartzokis, 2004b, 2004a; Dean et al., 2017; Yeatman et al., 2014), we found that myelination was likely the primary mechanism driving WM alterations in this cohort. Furthermore, we identified a distinct risk pattern in APOE4 carriers, where LDL-cholesterol was detrimental only in carriers.

4.1 Sex-related effects

In our sex-disaggregated analysis, we found that in both males and females, high systolic blood pressure, high BMI, high HbA1c (blood sugar levels), and low cholesterol (total, HDL, and LDL) were associated with low D2 (Fig 2, left panel). Due to the directions of relationships between risk factors and D2, we inferred that, in our analyses, greater D2 is likely to represent a healthier state. Since D2 represents the amount of deviation from the reference distribution (i.e., sex-balanced reference group), this would mean that higher D2 indicates WM microstructure that is healthier than the average of our reference group. Although the patterns of association were similar in males and females, the WM regions in which these relationships were observed differed between sexes (Fig 2, right panel), with partially overlapping significant clusters, but more frontal regions in males and more posterior and temporal locations in females. There was also a significant sex difference, where males expressed this general risk–WM pattern more strongly than females. There are several reports of sex differences in WM microstructure (Arshad et al., 2016; Kanaan et al., 2012; van Hemmen et al., 2017) and in the aging trajectory of myelin (Toschi et al., 2020). Age-related declines in WM health follow an anterior to posterior gradient, with females experiencing these changes later in life, likely owing to the pro-myelinating effects of female hormones (Bartzokis, 2004b; Toschi et al., 2020). However, the loss of this protective hormonal effect after menopause has been proposed as a key driver of the rapid WM deterioration observed post-menopause (Bartzokis, 2004b). Considering that the females in this study were well beyond the menopausal transition (median age at time of study = 67.27), they may be further along in the trajectory of age-related WM decline. This interpretation is in line with the spatial patterns observed here. However, the cross-sectional design of this study does not allow us to directly assess these trajectories or evaluate the influence of cardiovascular risk factors over time. Longitudinal analyses would be needed to fully explore these effects. Further research is also needed to better understand sex-specific relationships between cardiovascular risk factors and WM health, the potential impact of hormone replacement treatment, and the role of gender (Dhamala et al., 2024), which may confound these relationships.

The directions of several of the associations we found between WM D2 and risk factors are in line with the literature. Several studies report WM alterations in hypertensive individuals and the effects of high blood pressure may start accumulating as early as the fourth decade of life (Maillard et al., 2012). Obesity has also been associated with changes in WM microstructure such as decreased FA and myelin content (R1) in several WM tracts (Kullmann et al., 2015, 2016). In line with the extant literature on subclinical hyperglycemia (Garfield et al., 2021; Repple et al., 2021), we also identified WM differences associated with HbA1c levels, even though the vast majority of participants did not have diabetes (99% of females and 92% of males). Moreover, HDL cholesterol was positively associated with WM D2, in line with the well-established protective role of HDL on cognition and brain structure (Vitali et al., 2014).

4.2 APOE4-dependent effects of LDL

We found complex relationships between WM microstructure and LDL. Peripheral LDL and total cholesterol were positively associated with better WM health (high D2) in all but one latent variable. While LDL and total cholesterol are typically thought of as being detrimental, evidence on their impact on the brain's WM and on cognition is unclear (Alfaro et al., 2018; Lamar et al., 2020; Lv et al., 2016; Silverman & Schmeidler, 2018; van Vliet, 2012; Warstadt et al., 2014).

These discrepancies may be due to the unknown contribution of oxidized LDL to total LDL. Oxidation of LDL, which is enhanced in inflammatory states when oxidative stress is high, has been shown to be a better predictor of atherosclerosis and cardiovascular disease than LDL itself (Hecht & Harman, 2003; Holvoet et al., 2003, 2004; Nishi et al., 2002) and is also associated with deleterious effects on brain health (Dias et al., 2014; Draczynska-Lusiak et al., 1998). It is thus likely that the relationship we observed between LDL and WM was due to predominantly non-oxidized LDL. The fact that LDL and HDL cholesterol were related to WM D2 in the same direction also supports this hypothesis as the antioxidant property of HDL would contribute to preventing LDL oxidation (Holvoet et al., 2004; Sigurdardottir et al., 2002; Vitali et al., 2014). Furthermore, LDL oxidation may be reduced in the participants taking lipid-lowering medications as statins have been shown to reduce susceptibility of LDL to oxidation (Anderson et al., 1996; Ndrepepa et al., 2005; Vasankari et al., 2001).

In contrast, we found that high LDL was associated with poorer WM health in APOE4 carriers (LV2). This finding is consistent with a study reporting a detrimental effect of elevated LDL on WM microstructure in APOE4 carriers, but a beneficial effect in non-carriers (Ye et al., 2024). As a cholesterol-transporter, APOE4 may modulate the impact of LDL on WM microstructure through increased LDL circulation time, increased free radical formation and decreased plasma antioxidant concentrations, increasing LDL oxidation (Dias et al., 2014). The presence of two distinct patterns (i.e., LVs) in APOE4 carriers, one that differs from and one that is closer to non-carriers, may be due to other genes that impact lipid metabolism (Kunkle et al., 2019). Other genetic variants may thus counteract the effect of APOE4 on cholesterol metabolism and, consequently, on WM microstructure. The use of statins may also contribute to which pattern is expressed (Anderson et al., 1996; Ndrepepa et al., 2005; Vasankari et al., 2001). Overall, our study supports the idea of differential effects of LDL-cholesterol on the brain's WM depending on APOE genotype. However, future studies using more comprehensive genomic data and including measurements of oxidized LDL are needed to further explore these hypotheses.

The distinct pattern observed in APOE4 carriers (LV2), where low D2 was associated with high LDL, low HDL-cholesterol, high HbA1c, high BMI and high SBP, was found to be linked with cognition. D2 in a cluster of this LV was positively associated with immediate memory performance, indicating that this pattern of risk factors likely had a negative impact on cognition in APOE4 carriers. The direction of the relationship with cognition also supports our interpretation of low D2 reflecting poor WM health. On the other hand, in non-carriers, WM D2 in regions associated with risk factors did not relate with cognition. Together, our findings suggest that WM health is differentially affected by cardiometabolic risk factors in APOE4 carriers and that the pattern uncovered by LV2 may be more detrimental to cognitive health.

4.3 Role of myelin and other components

Several WM regions were associated with the patterns of risk factors discussed above and extracting the contribution of each MRI feature to D2 in these regions revealed that inter-individual variations in R1 and MTsat were major contributors in most significant clusters. This suggests that our findings were mainly driven by differences in myelin content, as both of these MRI features correlate strongly with macromolecular content and myelin (Callaghan et al., 2014; Draganski et al., 2011; Helms, Dathe, Kallenberg, et al., 2008). Our results are partially in line with the myelin breakdown theory stating that late-myelinating WM tracts would be especially vulnerable to aging and adverse risk factors such as those investigated in this study (Bartzokis, 2004a, 2011; Bartzokis et al., 2003, 2004; Burzynska et al., 2023; Dean et al., 2017; Foley et al., 2014). For instance, decreased FA in late-myelinating tracts has been reported in individuals with elevated glycated hemoglobin (HbA1c) (Foley et al., 2014). Similarly, decreased myelin water fraction, a robust measure of myelin, and R1 in those regions were found in a cohort of cognitively healthy middle-aged adults enriched for AD (Dean et al., 2017). Most of our significant clusters were located in late-myelinating regions (i.e., supramarginal, superior frontal, superior parietal, superior temporal, and precuneus WM), but we also found significant associations in the splenium of the corpus callosum, a region that develops at an intermediate stage (Bartzokis et al., 2003; Bartzokis, 2004a; Bartzokis et al., 2004; Bartzokis, 2011; Foley et al., 2014).

4.4 Strengths and limitations

In this study, we assessed relationships between risk factors and WM microstructure separately in each sex and APOE4 group, which allowed the identification of patterns specific to APOE4 carriers. Importantly, this pattern would not have been detected in a whole sample analysis (see Supplementary Fig 1 and Table 1). Another strength of our study is the use of a multivariate approach to integrate several MRI measures of WM, allowing for a comprehensive assessment of the biological mechanisms underlying WM differences (Tremblay et al., 2024). This multivariate integration is particularly relevant because multiple pathological mechanisms (e.g., demyelination, axonal changes, iron accumulation) are likely involved concurrently in AD and in its prodromal stage (Iturria-Medina et al., 2017). Our approach can also be useful for hypothesis generation, for instance to identify biological mechanisms or MRI features that are worth further investigation. Here, we identified differences in myelination as a likely mechanism. Future studies should use models that are more specific to myelin, such as myelin water imaging, to improve upon the limited specificity of the models used here (i.e., MTsat and R1) (Faulkner et al., 2024; MacKay & Laule, 2016). Methods have also been proposed to overcome the limitations of NODDI which tends to overestimate the cerebrospinal fluid and intracellular water fractions (Alsameen et al., 2023).

However, the D2 method has some inherent limitations. Because D2 is a squared measure, the directionality of differences is non-specific (Tremblay et al., 2024). Future studies could address this limitation by integrating models of ground-truth biophysical properties to better interpret these differences, or by stratifying groups based on the expected direction of change to have a strong prior on the directions of deviations. Further, the high sensitivity of D2 makes it susceptible to registration inaccuracies and partial voluming. Special attention must thus be paid to optimize alignment and minimize partial voluming. In this study, strict masking (i.e., 0.99 of group average tissue segmentation) was applied to restrict the analyses to voxels containing only WM. Another limitation of this study is that the sample size did not allow the investigation of a dose-dependent effect of the number of APOE $\boldsymbol{\varepsilon}$4 alleles. Future studies with larger samples and complete genomic data could help clarify the effects of the APOE genotype and other genes on cholesterol metabolism and the downstream impact on WM microstructure.

5. Conclusion

Our findings support the myelin breakdown hypothesis of AD, suggesting that oligodendrocytes' vulnerability to aging and various stressors makes myelin an early target in AD's pathology (Bartzokis, 2004a, 2011). Modifiable risk factors for AD (e.g., hypertension, diabetes, dyslipidemia) act as stressors that negatively impact WM health and cognition, especially when combined with familial history and APOE4. We found that WM microstructural alterations, likely reflecting variations in myelination, were associated with cardiometabolic risk factors in older adults with a family history of AD. Notably, LDL-cholesterol adversely affected WM microstructure only in APOE4 carriers. Our results also suggest that these WM alterations lead to impaired cognition, particularly short-term memory, in APOE4 carriers. Overall, our findings align with the theory that genetic and environmental risk factors exacerbate myelin breakdown and accelerate cognitive decline (Bartzokis, 2004a, 2011; Burzynska et al., 2023).

Author Contributions

Stefanie A Tremblay: Writing - Original Draft, Writing - Review & Editing, Formal analysis, Conceptualization, Methodology, Software, Visualization

R. Nathan Spreng: Funding acquisition, Resources, Writing - Review & Editing

Alfie Wearn: Formal analysis, Visualization, Writing - Review & Editing

Zaki Alasmar: Methodology, Software, Writing - Review & Editing, Conceptualization

Amir Pirhadi: Software, Methodology

Christine L. Tardif: Writing - Review & Editing, Methodology

Mallar M. Chakravarty: Methodology, Investigation

Sylvia Villeneuve: Funding acquisition, Investigation, Resources, Writing - Review & Editing

Ilana R. Leppert: Software, Methodology, Investigation

Felix Carbonell: Methodology

Yasser Iturria-Medina: Methodology, Writing - Review & Editing, Conceptualization, Funding acquisition

Christopher J Steele: Methodology, Conceptualization, Writing - Review & Editing, Software, Funding acquisition

Claudine J Gauthier: Supervision, Conceptualization, Writing - Review & Editing, Funding acquisition

Funding

This study was supported by the Canadian Institutes of Health Research (FRN: 175862, to Stefanie A. Tremblay), the Canadian Natural Sciences and Engineering Research Council (RGPIN-2015-04665, to Claudine J. Gauthier), the Michal and Renata Hornstein Chair in Cardiovascular Imaging (to Claudine J. Gauthier) and the Natural Sciences and Engineering Research Council of Canada Discovery (2024-06455, to Claudine J. Gauthier). Christopher J. Steele has received funding from the Natural Sciences and Engineering Research Council (NSERC: RGPIN-2020-06812, DGECR-2020-00146), the Heart and Stroke Foundation of Canada New Investigator Award and Catalyst from the Canadian Institutes of Health Research (HNC 170723), and the Fonds de Recherche Santé Chercheurs-boursier (FRQS CB Junior 2 349443). Christopher J. Steele and Yasser Iturria-Medina were also supported by the Quebec Bioimaging Network. R. Nathan Spreng is a Research Scholar supported by the Fonds de la Recherche du Quebec – Santé (FRQS). Alfie Wearn is a postdoctoral fellow also supported by FRQS.

Disclosures

The authors have no competing interests to declare.

Acknowledgments

We would like to acknowledge the PREVENT-AD research group who collected this dataset. The Founders of the program were John C. S. Breitner, MD, MPH, Judes Poirier, PhD and Pierre Etienne, MD, Douglas Hospital Research Centre and Faculty of Medicine, McGill University, Montréal, QC, Canada. Program Current Director is Sylvia Villeneuve, PhD, the Co-Director is

Judes Poirier, PhD and the Study Coordinator is Jennifer Tremblay-Mercier, MSc. PREVENT-AD is the result of efforts of many other co-investigators from a range of academic institutions and private corporations, as well as an extraordinarily dedicated and talented clinical and technical assistant staff, students, and post-doctoral fellows. Christine L. Tardif, Ilana R. Leppert, Sylvia Villeneuve, and R. Nathan Spreng are authors affiliated with the PREVENT-AD research team. We would also like to thank the study participants who were recruited from the greater Montréal area and more distant locations in Québec. For up-to-date information, see https://prevent-alzheimer.net/?page_id=42&lang=en.

References

Adluru, N., Destiche, D. J., Lu, S. Y.-F., Doran, S. T., Birdsill, A. C., Melah, K. E., Okonkwo, O. C., Alexander, A. L., Dowling, N. M., Johnson, S. C., Sager, M. A., & Bendlin, B. B. (2014). White matter microstructure in late middle-age: Effects of apolipoprotein E4 and parental family history of Alzheimer's disease. *NeuroImage: Clinical*, *4*, 730–742. https://doi.org/10.1016/j.nicl.2014.04.008

Agosta, F., Pievani, M., Sala, S., Geroldi, C., Galluzzi, S., Frisoni, G. B., & Filippi, M. (2011). White Matter Damage in Alzheimer Disease and Its Relationship to Gray Matter Atrophy. *Radiology*, *258*(3), 853–863. https://doi.org/10.1148/radiol.10101284

Alasmar, Z., Tremblay, S. A., Baumeister, T. R., Carbonell, F., Iturria-Medina, Y., Gauthier, C. J., & Steele, C. J. (2024). *White Matter Microstructural Correlates of Cognitive and Motor Functioning Revealed via Multimodal Multivariate Analysis* (p. 2024.06.05.597645). bioRxiv. https://doi.org/10.1101/2024.06.05.597645

Alfaro, F. J., Gavrieli, A., Saade-Lemus, P., Lioutas, V.-A., Upadhyay, J., & Novak, V. (2018). White matter microstructure and cognitive decline in metabolic syndrome: A review of diffusion tensor imaging. *Metabolism*, *78*, 52–68. https://doi.org/10.1016/j.metabol.2017.08.009

Alsameen, M. H., Gong, Z., Qian, W., Kiely, M., Triebswetter, C., Bergeron, C. M., Cortina, L. E., Faulkner, M. E., Laporte, J. P., & Bouhrara, M. (2023). C-NODDI: A constrained NODDI model for axonal density and orientation determinations in cerebral white matter. *Frontiers in Neurology*, *14*. https://doi.org/10.3389/fneur.2023.1205426

Altmann, A., Tian, L., Henderson, V. W., Greicius, M. D., & Investigators, A. D. N. I. (2014). Sex modifies the APOE-related risk of developing Alzheimer disease. *Annals of Neurology*, *75*(4), 563–573. https://doi.org/10.1002/ana.24135

Anderson, T. J., Meredith, I. T., Charbonneau, F., Yeung, A. C., Frei, B., Selwyn, A. P., & Ganz, P. (1996). Endothelium-Dependent Coronary Vasomotion Relates to the Susceptibility of LDL to Oxidation in Humans. *Circulation*, *93*(9), 1647–1650. https://doi.org/10.1161/01.CIR.93.9.1647

Araque Caballero, M. Á., Suárez-Calvet, M., Duering, M., Franzmeier, N., Benzinger, T., Fagan, A. M., Bateman, R. J., Jack, C. R., Levin, J., Dichgans, M., Jucker, M., Karch, C., Masters, C. L., Morris, J. C., Weiner, M., Rossor, M., Fox, N. C., Lee, J.-H., Salloway, S., … Ewers, M. (2018). White matter diffusion alterations precede symptom onset in autosomal dominant Alzheimer's disease. *Brain*, *141*(10), 3065–3080. https://doi.org/10.1093/brain/awy229

Arshad, M., Stanley, J. A., & Raz, N. (2016). Adult Age Differences in Subcortical Myelin Content Are Consistent with Protracted Myelination and Unrelated to Diffusion Tensor Imaging Indices. *NeuroImage*, *143*, 26–39. https://doi.org/10.1016/j.neuroimage.2016.08.047

Barnes, J., Bartlett, J. W., van de Pol, L. A., Loy, C. T., Scahill, R. I., Frost, C., Thompson, P., & Fox, N. C. (2009). A meta-analysis of hippocampal atrophy rates in Alzheimer's disease. *Neurobiology of Aging*, *30*(11), 1711–1723. https://doi.org/10.1016/j.neurobiolaging.2008.01.010

Bartzokis, G. (2004a). Age-related myelin breakdown: A developmental model of cognitive decline and Alzheimer's disease. *Neurobiology of Aging*, *25*(1), 5–18. https://doi.org/10.1016/j.neurobiolaging.2003.03.001

Bartzokis, G. (2004b). Quadratic trajectories of brain myelin content: Unifying construct for neuropsychiatric disorders. *Neurobiology of Aging*, *25*(1), 49–62. https://doi.org/10.1016/j.neurobiolaging.2003.08.001

Bartzokis, G. (2011). Alzheimer's disease as homeostatic responses to age-related myelin breakdown. *Neurobiology of Aging*, *32*(8), 1341–1371. https://doi.org/10.1016/j.neurobiolaging.2009.08.007

Bartzokis, G., Cummings, J. L., Sultzer, D., Henderson, V. W., Nuechterlein, K. H., & Mintz, J. (2003). White Matter Structural Integrity in Healthy Aging Adults and Patients With Alzheimer Disease: A Magnetic Resonance Imaging Study. *Archives of Neurology*, *60*(3), 393–398. https://doi.org/10.1001/archneur.60.3.393

Bartzokis, G., Sultzer, D., Lu, P. H., Nuechterlein, K. H., Mintz, J., & Cummings, J. L. (2004). Heterogeneous age-related breakdown of white matter structural integrity: Implications for cortical “disconnection” in aging and Alzheimer’s disease. *Neurobiology of Aging*, *25*(7), 843–851. https://doi.org/10.1016/j.neurobiolaging.2003.09.005

Basser, P. J., Mattiello, J., & LeBihan, D. (1994). MR diffusion tensor spectroscopy and imaging. *Biophysical Journal*, *66*(1), 259–267. https://doi.org/10.1016/S0006-3495(94)80775-1

Birdsill, A. C., Oleson, S., Kaur, S., Pasha, E., Ireton, A., Tanaka, H., & Haley, A. (2017). Abdominal obesity and white matter microstructure in midlife. *Human Brain Mapping*, *38*(7), 3337–3344. https://doi.org/10.1002/hbm.23576

Breitner, J. C. S., Wyse, B. W., Anthony, J. C., Welsh-Bohmer, K. A., Steffens, D. C., Norton, M. C., Tschanz, J. T., Plassman, B. L., Meyer, M. R., Skoog, I., & Khachaturian, A. (1999). APOE-ε4 count predicts age when prevalence of AD increases, then declines. *Neurology*, *53*(2), 321–321. https://doi.org/10.1212/WNL.53.2.321

Burzynska, A. Z., Anderson, C., Arciniegas, D. B., Calhoun, V., Choi, I.-Y., Colmenares, A. M., Hiner, G., Kramer, A. F., Li, K., Lee, J., Lee, P., Oh, S.-H., Umland, S., & Thomas, M. L. (2023). Metabolic syndrome and adiposity: Risk factors for decreased myelin in cognitively healthy adults. *Cerebral Circulation - Cognition and Behavior*, *5*, 100180. https://doi.org/10.1016/j.cccb.2023.100180

Calamante, F., Smith, R. E., Tournier, J.-D., Raffelt, D., & Connelly, A. (2015). Quantification of voxel-wise total fibre density: Investigating the problems associated with track-count mapping. *NeuroImage*, *117*, 284–293. https://doi.org/10.1016/j.neuroimage.2015.05.070

Callaghan, M. F., Freund, P., Draganski, B., Anderson, E., Cappelletti, M., Chowdhury, R., Diedrichsen, J., FitzGerald, T. H. B., Smittenaar, P., Helms, G., Lutti, A., & Weiskopf, N.

(2014). Widespread age-related differences in the human brain microstructure revealed by quantitative magnetic resonance imaging. *Neurobiology of Aging*, *35*(8), 1862–1872. https://doi.org/10.1016/j.neurobiolaging.2014.02.008

Campbell, J. S., Leppert, I. R., Narayanan, S., Boudreau, M., Duval, T., Cohen-Adad, J., Pike, G. B., & Stikov, N. (2018). Promise and pitfalls of g-ratio estimation with MRI. *Neuroimage*, *182*, 80–96.

Chen, J.-F., Liu, K., Hu, B., Li, R.-R., Xin, W., Chen, H., Wang, F., Chen, L., Li, R.-X., Ren, S.-Y., Xiao, L., Chan, J. R., & Mei, F. (2021). Enhancing myelin renewal reverses cognitive dysfunction in a murine model of Alzheimer's disease. *Neuron*, *109*(14), 2292-2307.e5. https://doi.org/10.1016/j.neuron.2021.05.012

Chen, J.-F., Wang, F., Huang, N.-X., Xiao, L., & Mei, F. (2022). Oligodendrocytes and myelin: Active players in neurodegenerative brains? *Developmental Neurobiology*, *82*(2), 160–174. https://doi.org/10.1002/dneu.22867

Chung, S., Kim, D., Breton, E., & Axel, L. (2010). Rapid B1+ mapping using a preconditioning RF pulse with TurboFLASH readout. *Magnetic Resonance in Medicine*, *64*(2), 439–446. https://doi.org/10.1002/mrm.22423

Cleeman, J. (2001). *ATP III Guidelines At-A-Glance Quick Desk Reference*.

Daducci, A., Canales-Rodríguez, E. J., Zhang, H., Dyrby, T. B., Alexander, D. C., & Thiran, J.-P. (2015). Accelerated Microstructure Imaging via Convex Optimization (AMICO) from diffusion MRI data. *NeuroImage*, *105*, 32–44. https://doi.org/10.1016/j.neuroimage.2014.10.026

Dean, D. C., III, Hurley, S. A., Kecskemeti, S. R., O'Grady, J. P., Canda, C., Davenport-Sis, N. J., Carlsson, C. M., Zetterberg, H., Blennow, K., Asthana, S., Sager, M. A., Johnson, S. C., Alexander, A. L., & Bendlin, B. B. (2017). Association of Amyloid Pathology With Myelin Alteration in Preclinical Alzheimer Disease. *JAMA Neurology*, *74*(1), 41–49. https://doi.org/10.1001/jamaneurol.2016.3232

Dean, D. C., Jerskey, B. A., Chen, K., Protas, H., Thiyyagura, P., Roontiva, A., O'Muircheartaigh, J., Dirks, H., Waskiewicz, N., Lehman, K., Siniard, A. L., Turk, M. N., Hua, X., Madsen, S. K., Thompson, P. M., Fleisher, A. S., Huentelman, M. J., Deoni, S. C. L., & Reiman, E. M. (2014). Brain Differences in Infants at Differential Genetic Risk for Late-Onset Alzheimer Disease A Cross-sectional Imaging Study. *JAMA Neurology*, *71*(1), 11–22. https://doi.org/10.1001/jamaneurol.2013.4544

Dell'Acqua, F., & Tournier, J.-D. (2019). Modelling white matter with spherical deconvolution: How and why? *NMR in Biomedicine*, *32*(4), e3945. https://doi.org/10.1002/nbm.3945

Desai, M. K., Sudol, K. L., Janelsins, M. C., Mastrangelo, M. A., Frazer, M. E., & Bowers, W. J. (2009). Triple-transgenic Alzheimer's disease mice exhibit region-specific abnormalities in brain myelination patterns prior to appearance of amyloid and tau pathology. *Glia*, *57*(1), 54–65. https://doi.org/10.1002/glia.20734

Dhamala, E., Bassett, D. S., Yeo, B. T., & Holmes, A. J. (2024). Functional brain networks are associated with both sex and gender in children. *Science Advances*, *10*(28), eadn4202. https://doi.org/10.1126/sciadv.adn4202

Dias, I. H. K., Polidori, M. C., & Griffiths, H. R. (2014). Hypercholesterolaemia-induced oxidative stress at the blood–brain barrier. *Biochemical Society Transactions*, *42*(4), 1001–1005. https://doi.org/10.1042/BST20140164

Draczynska-Lusiak, B., Doung, A., & Sun, A. Y. (1998). Oxidized lipoproteins may play a role in neuronal cell death in Alzheimer disease. *Molecular and Chemical Neuropathology*, *33*(2), 139–148. https://doi.org/10.1007/BF02870187

Draganski, B., Ashburner, J., Hutton, C., Kherif, F., Frackowiak, R. S. J., Helms, G., & Weiskopf, N. (2011). Regional specificity of MRI contrast parameter changes in normal ageing revealed by voxel-based quantification (VBQ). *NeuroImage*, *55*(4), 1423–1434. https://doi.org/10.1016/j.neuroimage.2011.01.052

Duff, K., Hobson, V. L., Beglinger, L. J., & O'Bryant, S. E. (2010). Diagnostic Accuracy of the RBANS in Mild Cognitive Impairment: Limitations on Assessing Milder Impairments. *Archives of Clinical Neuropsychology*, *25*(5), 429–441. https://doi.org/10.1093/arclin/acq045

Farrer, L. A., Cupples, L. A., Haines, J. L., Hyman, B., Kukull, W. A., Mayeux, R., Myers, R. H., Pericak-Vance, M. A., Risch, N., & van Duijn, C. M. (1997). Effects of Age, Sex, and Ethnicity on the Association Between Apolipoprotein E Genotype and Alzheimer Disease: A Meta-analysis. *JAMA*, *278*(16), 1349–1356. https://doi.org/10.1001/jama.1997.03550160069041

Faulkner, M. E., Gong, Z., Guo, A., Laporte, J. P., Bae, J., & Bouhrara, M. (2024). Harnessing myelin water fraction as an imaging biomarker of human cerebral aging, neurodegenerative diseases, and risk factors influencing myelination: A review. *Journal of Neurochemistry*, *168*(9), 2243–2263. https://doi.org/10.1111/jnc.16170

Foley, J. M., Salat, D. H., Stricker, N. H., Zink, T. A., Grande, L. J., McGlinchey, R. E., Milberg, W. P., & Leritz, E. C. (2014). Interactive Effects of Apolipoprotein E4 and Diabetes Risk on Later Myelinating White Matter Regions in Neurologically Healthy Older Aged Adults. *American Journal of Alzheimer's Disease & Other Dementias®*, *29*(3), 222–235. https://doi.org/10.1177/1533317513517045

Garfield, V., Farmaki, A.-E., Eastwood, S. V., Mathur, R., Rentsch, C. T., Bhaskaran, K., Smeeth, L., & Chaturvedi, N. (2021). HbA1c and brain health across the entire glycaemic spectrum. *Diabetes, Obesity and Metabolism*, *23*(5), 1140–1149. https://doi.org/10.1111/dom.14321

Goldberg, T. E., Huey, E. D., & Devanand, D. P. (2020). Association of APOE e2 genotype with Alzheimer's and non-Alzheimer's neurodegenerative pathologies. *Nature Communications*, *11*(1), 4727. https://doi.org/10.1038/s41467-020-18198-x

Gong, Z., Bilgel, M., Kiely, M., Triebswetter, C., Ferrucci, L., Resnick, S. M., Spencer, R. G., & Bouhrara, M. (2023). Lower myelin content is associated with more rapid cognitive decline among cognitively unimpaired individuals. *Alzheimer's & Dementia : The Journal of the Alzheimer's Association*, *19*(7), 3098–3107. https://doi.org/10.1002/alz.12968

Hecht, H. S., & Harman, S. M. (2003). Relation of aggressiveness of lipid-lowering treatment to changes in calcified plaque burden by electron beam tomography. *The American Journal of Cardiology*, *92*(3), 334–336. https://doi.org/10.1016/S0002-9149(03)00642-8

Helms, G., Dathe, H., & Dechent, P. (2008). Quantitative FLASH MRI at 3T using a rational approximation of the Ernst equation. *Magnetic Resonance in Medicine*, *59*(3), 667–672. https://doi.org/10.1002/mrm.21542

Helms, G., Dathe, H., Kallenberg, K., & Dechent, P. (2008). High-resolution maps of magnetization transfer with inherent correction for RF inhomogeneity and T1 relaxation obtained from 3D FLASH MRI. *Magnetic Resonance in Medicine: An Official Journal of the International Society for Magnetic Resonance in Medicine*, *60*(6), 1396–1407.

Holvoet, P., Harris, T. B., Tracy, R. P., Verhamme, P., Newman, A. B., Rubin, S. M., Simonsick, E. M., Colbert, L. H., & Kritchevsky, S. B. (2003). Association of High Coronary Heart Disease Risk Status With Circulating Oxidized LDL in the Well-Functioning Elderly. *Arteriosclerosis, Thrombosis, and Vascular Biology*, *23*(8), 1444–1448. https://doi.org/10.1161/01.ATV.0000080379.05071.22

Holvoet, P., Kritchevsky, S. B., Tracy, R. P., Mertens, A., Rubin, S. M., Butler, J., Goodpaster, B., & Harris, T. B. (2004). The Metabolic Syndrome, Circulating Oxidized LDL, and Risk of Myocardial Infarction in Well-Functioning Elderly People in the Health, Aging, and Body Composition Cohort. *Diabetes*, *53*(4), 1068–1073. https://doi.org/10.2337/diabetes.53.4.1068

Huang, W., Qiu, C., von Strauss, E., Winblad, B., & Fratiglioni, L. (2004). APOE Genotype, Family History of Dementia, and Alzheimer Disease Risk: A 6-Year Follow-up Study. *Archives of Neurology*, *61*(12), 1930–1934. https://doi.org/10.1001/archneur.61.12.1930

Iturria-Medina, Y., Carbonell, F. M., Sotero, R. C., Chouinard-Decorte, F., & Evans, A. C. (2017). Multifactorial causal model of brain (dis)organization and therapeutic intervention: Application to Alzheimer's disease. *NeuroImage*, *152*, 60–77. https://doi.org/10.1016/j.neuroimage.2017.02.058

Jeurissen, B., Tournier, J.-D., Dhollander, T., Connelly, A., & Sijbers, J. (2014). Multi-tissue constrained spherical deconvolution for improved analysis of multi-shell diffusion MRI data. *NeuroImage*, *103*, 411–426. https://doi.org/10.1016/j.neuroimage.2014.07.061

Kanaan, R. A., Allin, M., Picchioni, M., Barker, G. J., Daly, E., Shergill, S. S., Woolley, J., & McGuire, P. K. (2012). Gender Differences in White Matter Microstructure. *PLoS ONE*, *7*(6), e38272. https://doi.org/10.1371/journal.pone.0038272

Karakaya, J., Akin, S., Karagaoglu, E., & Gurlek, A. (2014). The performance of hemoglobin A1c against fasting plasma glucose and oral glucose tolerance test in detecting prediabetes and diabetes. *Journal of Research in Medical Sciences : The Official Journal of Isfahan University of Medical Sciences*, *19*(11), 1051–1057.

Kiely, M., Triebswetter, C., Cortina, L. E., Gong, Z., Alsameen, M. H., Spencer, R. G., & Bouhrara, M. (2022). Insights into human cerebral white matter maturation and degeneration across the adult lifespan. *NeuroImage*, *247*, 118727. https://doi.org/10.1016/j.neuroimage.2021.118727

Kullmann, S., Callaghan, M. F., Heni, M., Weiskopf, N., Scheffler, K., Häring, H.-U., Fritsche, A., Veit, R., & Preissl, H. (2016). Specific white matter tissue microstructure changes associated with obesity. *NeuroImage*, *125*, 36–44. Scopus. https://doi.org/10.1016/j.neuroimage.2015.10.006

Kullmann, S., Schweizer, F., Veit, R., Fritsche, A., & Preissl, H. (2015). Compromised white matter integrity in obesity. *Obesity Reviews*, *16*(4), 273–281. https://doi.org/10.1111/obr.12248

Kunkle, B. W., Grenier-Boley, B., Sims, R., Bis, J. C., Damotte, V., Naj, A. C., Boland, A., Vronskaya, M., van der Lee, S. J., Amlie-Wolf, A., Bellenguez, C., Frizatti, A., Chouraki, V., Martin, E.

R., Sleegers, K., Badarinarayan, N., Jakobsdottir, J., Hamilton-Nelson, K. L., Moreno-Grau, S., … Pericak-Vance, M. A. (2019). Genetic meta-analysis of diagnosed Alzheimer's disease identifies new risk loci and implicates Aβ, tau, immunity and lipid processing. *Nature Genetics*, *51*(3), 414–430. https://doi.org/10.1038/s41588-019-0358-2

Lamar, M., Durazo-Arvizu, R. A., Rodriguez, C. J., Kaplan, R. C., Perera, M. J., Cai, J., Giacinto, R. A. E., González, H. M., & Daviglus, M. L. (2020). Associations of Lipid Levels and Cognition: Findings from the Hispanic Community Health Study/Study of Latinos. *Journal of the International Neuropsychological Society*, *26*(3), 251–262. https://doi.org/10.1017/S1355617719001000

Livingston, G., Huntley, J., Liu, K. Y., Costafreda, S. G., Selbæk, G., Alladi, S., Ames, D., Banerjee, S., Burns, A., Brayne, C., Fox, N. C., Ferri, C. P., Gitlin, L. N., Howard, R., Kales, H. C., Kivimäki, M., Larson, E. B., Nakasujja, N., Rockwood, K., … Mukadam, N. (2024). Dementia prevention, intervention, and care: 2024 report of the Lancet standing Commission. *The Lancet*, *0*(0). https://doi.org/10.1016/S0140-6736(24)01296-0

Lv, Y.-B., Yin, Z. X., Chei, C.-L., Brasher, M. S., Zhang, J., Kraus, V. B., Qian, F., Shi, X., Matchar, D. B., & Zeng, Y. (2016). Serum cholesterol levels within the high normal range are associated with better cognitive performance among Chinese elderly. *The Journal of Nutrition, Health and Aging*, *20*(3), 280–287. https://doi.org/10.1007/s12603-016-0701-6

MacKay, A. L., & Laule, C. (2016). Magnetic Resonance of Myelin Water: An in vivo Marker for Myelin. *Brain Plasticity*, *2*(1), 71–91. https://doi.org/10.3233/BPL-160033

Mahalanobis, P. C. (1936). *On the generalized distance in statistics*.

Maier-Hein, K. H., Westin, C.-F., Shenton, M. E., Weiner, M. W., Raj, A., Thomann, P., Kikinis, R., Stieltjes, B., & Pasternak, O. (2015). Widespread white matter degeneration preceding the onset of dementia. *Alzheimer's & Dementia*, *11*(5), 485-493.e2. https://doi.org/10.1016/j.jalz.2014.04.518

Maillard, P., Seshadri, S., Beiser, A., Himali, J. J., Au, R., Fletcher, E., Carmichael, O., Wolf, P. A., & DeCarli, C. (2012). Effects of systolic blood pressure on white-matter integrity in young adults in the Framingham Heart Study: A cross-sectional study. *The Lancet Neurology*, *11*(12), 1039–1047. https://doi.org/10.1016/S1474-4422(12)70241-7

McIntosh, A. R., & Lobaugh, N. J. (2004). Partial least squares analysis of neuroimaging data: Applications and advances. *NeuroImage*, *23 Suppl 1*, S250-263. https://doi.org/10.1016/j.neuroimage.2004.07.020

Mole, J. P., Fasano, F., Evans, J., Sims, R., Hamilton, D. A., Kidd, E., & Metzler-Baddeley, C. (2020). Genetic risk of dementia modifies obesity effects on white matter myelin in cognitively healthy adults. *Neurobiology of Aging*, *94*, 298–310. https://doi.org/10.1016/j.neurobiolaging.2020.06.014

Nasrabady, S. E., Rizvi, B., Goldman, J. E., & Brickman, A. M. (2018). White matter changes in Alzheimer's disease: A focus on myelin and oligodendrocytes. *Acta Neuropathologica Communications*, *6*(1), 22. https://doi.org/10.1186/s40478-018-0515-3

Ndrepepa, G., Braun, S., von Beckerath, N., Mehilli, J., Gorchakova, O., Vogt, W., Schömig, A., & Kastrati, A. (2005). Oxidized low density lipoproteins, statin therapy and severity of coronary artery disease. *Clinica Chimica Acta*, *360*(1), 178–186. https://doi.org/10.1016/j.cccn.2005.04.032

Nishi, K., Itabe, H., Uno, M., Kitazato, K. T., Horiguchi, H., Shinno, K., & Nagahiro, S. (2002). Oxidized LDL in Carotid Plaques and Plasma Associates With Plaque Instability. *Arteriosclerosis, Thrombosis, and Vascular Biology*, *22*(10), 1649–1654. https://doi.org/10.1161/01.ATV.0000033829.14012.18

Parrilla, G. E., Gupta, V., Wall, R. V., Salkar, A., Basavarajappa, D., Mirzaei, M., Chitranshi, N., Graham, S. L., & You, Y. (2024). The role of myelin in neurodegeneration: Implications for drug targets and neuroprotection strategies. *Reviews in the Neurosciences*, *35*(3), 271–292. https://doi.org/10.1515/revneuro-2023-0081

Raffelt, D., Dhollander, T., Tournier, J.-D., Tabbara, R., Smith, R. E., Pierre, E., & Connelly, A. (2017). Bias Field Correction and Intensity Normalisation for Quantitative Analysis of Apparent Fibre Density. *In Proc. ISMRM*.

Raffelt, D., Tournier, J.-D., Fripp, J., Crozier, S., Connelly, A., & Salvado, O. (2011). Symmetric diffeomorphic registration of fibre orientation distributions. *NeuroImage*, *56*(3), 1171–1180. https://doi.org/10.1016/j.neuroimage.2011.02.014

Raffelt, D., Tournier, J.-D., Rose, S., Ridgway, G. R., Henderson, R., Crozier, S., Salvado, O., & Connelly, A. (2012). Apparent Fibre Density: A novel measure for the analysis of diffusion-weighted magnetic resonance images. *NeuroImage*, *59*(4), 3976–3994. https://doi.org/10.1016/j.neuroimage.2011.10.045

Raffelt, D., Tournier, J.-D., Smith, R. E., Vaughan, D. N., Jackson, G., Ridgway, G. R., & Connelly, A. (2017). Investigating white matter fibre density and morphology using fixel-based analysis. *NeuroImage*, *144*, 58–73. https://doi.org/10.1016/j.neuroimage.2016.09.029

Randolph, C., Tierney, M. C., Mohr, E., & Chase, T. N. (1998). The Repeatable Battery for the Assessment of Neuropsychological Status (RBANS): Preliminary Clinical Validity. *Journal of Clinical and Experimental Neuropsychology*, *20*(3), 310–319. https://doi.org/10.1076/jcen.20.3.310.823

Remer, J., Dean, D. C., Chen, K., Reiman, R. A., Huentelman, M. J., Reiman, E. M., & Deoni, S. C. L. (2020). Longitudinal white matter and cognitive development in pediatric carriers of the apolipoprotein ε4 allele. *Neuroimage*, *222*, 117243. https://doi.org/10.1016/j.neuroimage.2020.117243

Repple, J., Karliczek, G., Meinert, S., Förster, K., Grotegerd, D., Goltermann, J., Redlich, R., Arolt, V., Baune, B. T., Dannlowski, U., & Opel, N. (2021). Variation of HbA1c affects cognition and white matter microstructure in healthy, young adults. *Molecular Psychiatry*, *26*(4), 1399–1408. https://doi.org/10.1038/s41380-019-0504-3

Riffert, T. W., Schreiber, J., Anwander, A., & Knösche, T. R. (2014). Beyond fractional anisotropy: Extraction of bundle-specific structural metrics from crossing fiber models. *NeuroImage*, *100*, 176–191. https://doi.org/10.1016/j.neuroimage.2014.06.015

Shobab, L. A., Hsiung, G.-Y. R., & Feldman, H. H. (2005). Cholesterol in Alzheimer's disease. *Lancet Neurology*, *4*(12), 841–852. Scopus. https://doi.org/10.1016/S1474-4422(05)70248-9

Sigurdardottir, V., Fagerberg, B., & Hulthe, J. (2002). Circulating oxidized low-density lipoprotein (LDL) is associated with risk factors of the metabolic syndrome and LDL size in clinically healthy 58-year-old men (AIR study). *Journal of Internal Medicine*, *252*(5), 440–447. https://doi.org/10.1046/j.1365-2796.2002.01054.x

Silverman, J. M., & Schmeidler, J. (2018). Outcome age-based prediction of successful cognitive aging by total cholesterol. *Alzheimer's & Dementia*, *14*(7), 952–960. https://doi.org/10.1016/j.jalz.2018.01.009

Smith, R. E., Tournier, J.-D., Calamante, F., & Connelly, A. (2012). Anatomically-constrained tractography: Improved diffusion MRI streamlines tractography through effective use of anatomical information. *NeuroImage*, *62*(3), 1924–1938. https://doi.org/10.1016/j.neuroimage.2012.06.005

Smith, R. E., Tournier, J.-D., Calamante, F., & Connelly, A. (2013). SIFT: Spherical-deconvolution informed filtering of tractograms. *NeuroImage*, *67*, 298–312. https://doi.org/10.1016/j.neuroimage.2012.11.049

Subramaniapillai, S., Rajagopal, S., Snytte, J., Otto, A. R., PREVENT-AD Research Group, Einstein, G., & Rajah, M. N. (2021). Sex differences in brain aging among adults with family history of Alzheimer's disease and APOE4 genetic risk. *NeuroImage. Clinical*, *30*, 102620. https://doi.org/10.1016/j.nicl.2021.102620

Tabelow, K., Balteau, E., Ashburner, J., Callaghan, M. F., Draganski, B., Helms, G., Kherif, F., Leutritz, T., Lutti, A., Phillips, C., Reimer, E., Ruthotto, L., Seif, M., Weiskopf, N., Ziegler, G., & Mohammadi, S. (2019). hMRI - A toolbox for quantitative MRI in neuroscience and clinical research. *NeuroImage*, *194*, 191–210. https://doi.org/10.1016/j.neuroimage.2019.01.029

Tardif, C. L., Gauthier, C. J., Steele, C. J., Bazin, P.-L., Schäfer, A., Schaefer, A., Turner, R., & Villringer, A. (2016). Advanced MRI techniques to improve our understanding of experience-induced neuroplasticity. *Neuroimage*, *131*, 55–72.

Tian, J., Raghavan, S., Reid, R. I., Przybelski, S. A., Lesnick, T. G., Gebre, R. K., Graff-Radford, J., Schwarz, C. G., Lowe, V. J., Kantarci, K., Knopman, D. S., Petersen, R. C., Jack, C. R., & Vemuri, P. (2023). White Matter Degeneration Pathways Associated With Tau Deposition in Alzheimer Disease. *Neurology*, *100*(22), e2269–e2278. https://doi.org/10.1212/WNL.0000000000207250

Toschi, N., Gisbert, R. A., Passamonti, L., Canals, S., & De Santis, S. (2020). Multishell diffusion imaging reveals sex-specific trajectories of early white matter degeneration in normal aging. *Neurobiology of Aging*, *86*, 191–200. https://doi.org/10.1016/j.neurobiolaging.2019.11.014

Tournier, J.-D., Smith, R., Raffelt, D., Tabbara, R., Dhollander, T., Pietsch, M., Christiaens, D., Jeurissen, B., Yeh, C.-H., & Connelly, A. (2019). MRtrix3: A fast, flexible and open software framework for medical image processing and visualisation. *NeuroImage*, 116137.

Tremblay, S. A., Alasmar, Z., Pirhadi, A., Carbonell, F., Iturria-Medina, Y., Gauthier, C. J., & Steele, C. J. (2024). MVComp toolbox: MultiVariate Comparisons of brain MRI features accounting for common information across measures. *Aperture Neuro*, *4*. https://doi.org/10.52294/001c.118427

Tremblay-Mercier, J., Madjar, C., Das, S., Pichet Binette, A., Dyke, S. O. M., Étienne, P., Lafaille-Magnan, M.-E., Remz, J., Bellec, P., Louis Collins, D., Natasha Rajah, M., Bohbot, V., Leoutsakos, J.-M., Iturria-Medina, Y., Kat, J., Hoge, R. D., Gauthier, S., Tardif, C. L., Mallar Chakravarty, M., … Breitner, J. C. S. (2021). Open science datasets from PREVENT-AD, a longitudinal cohort of pre-symptomatic Alzheimer's disease. *NeuroImage: Clinical*, *31*, 102733. https://doi.org/10.1016/j.nicl.2021.102733

Triebswetter, C., Kiely, M., Khattar, N., Ferrucci, L., Resnick, S. M., Spencer, R. G., & Bouhrara, M. (2022). Differential associations between apolipoprotein E alleles and cerebral myelin content in normative aging. *NeuroImage*, *251*, 118988. https://doi.org/10.1016/j.neuroimage.2022.118988

Tustison, N. J., Avants, B. B., Cook, P. A., Yuanjie Zheng, Egan, A., Yushkevich, P. A., & Gee, J. C. (2010). N4ITK: Improved N3 Bias Correction. *IEEE Transactions on Medical Imaging*, *29*(6), 1310–1320. https://doi.org/10.1109/TMI.2010.2046908

van Hemmen, J., Saris, I. M. J., Cohen-Kettenis, P. T., Veltman, D. J., Pouwels, P. J. W., & Bakker, J. (2017). Sex Differences in White Matter Microstructure in the Human Brain Predominantly Reflect Differences in Sex Hormone Exposure. *Cerebral Cortex*, *27*(5), 2994–3001. https://doi.org/10.1093/cercor/bhw156

van Vliet, P. (2012). Cholesterol and late-life cognitive decline. *Journal of Alzheimer's Disease: JAD*, *30 Suppl 2*, S147-162. https://doi.org/10.3233/JAD-2011-111028

Vasankari, T., Ahotupa, M., Toikka, J., Mikkola, J., Irjala, K., Pasanen, P., Neuvonen, K., Raitakari, O., & Viikari, J. (2001). Oxidized LDL and thickness of carotid intima-media are associated with coronary atherosclerosis in middle-aged men: Lower levels of oxidized LDL with statin therapy. *Atherosclerosis*, *155*(2), 403–412. https://doi.org/10.1016/S0021-9150(00)00573-6

Vitali, C., Wellington, C. L., & Calabresi, L. (2014). HDL and cholesterol handling in the brain. *Cardiovascular Research*, *103*(3), 405–413. https://doi.org/10.1093/cvr/cvu148

Wang, R., Fratiglioni, L., Laukka, E. J., Lövdén, M., Kalpouzos, G., Keller, L., Graff, C., Salami, A., Bäckman, L., & Qiu, C. (2015). Effects of vascular risk factors and APOE ε4 on white matter integrity and cognitive decline. *Neurology*, *84*(11), 1128–1135. https://doi.org/10.1212/WNL.0000000000001379

Wang, W.-Y., Yu, J.-T., Liu, Y., Yin, R.-H., Wang, H.-F., Wang, J., Tan, L., Radua, J., & Tan, L. (2015). Voxel-based meta-analysis of grey matter changes in Alzheimer's disease. *Translational Neurodegeneration*, *4*(1), 6. https://doi.org/10.1186/s40035-015-0027-z

Warstadt, N. M., Dennis, E. L., Jahanshad, N., Kohannim, O., Nir, T. M., McMahon, K. L., de Zubicaray, G. I., Montgomery, G. W., Henders, A. K., Martin, N. G., Whitfield, J. B., Jack, C. R., Bernstein, M. A., Weiner, M. W., Toga, A. W., Wright, M. J., & Thompson, P. M. (2014). Serum cholesterol and variant in cholesterol-related gene *CETP* predict white matter microstructure. *Neurobiology of Aging*, *35*(11), 2504–2513. https://doi.org/10.1016/j.neurobiolaging.2014.05.024

Wearn, A., Tremblay, S. A., Tardif, C. L., Leppert, I. R., Gauthier, C. J., Baracchini, G., Hughes, C., Hewan, P., Tremblay-Mercier, J., Rosa-Neto, P., Poirier, J., Villeneuve, S., Schmitz, T. W., Turner, G. R., & Spreng, R. N. (2024). Neuromodulatory subcortical nucleus integrity is associated with white matter microstructure, tauopathy and APOE status. *Nature Communications*, *15*(1), 4706. https://doi.org/10.1038/s41467-024-48490-z

Weiskopf, N., Suckling, J., Williams, G., Correia, M. M., Inkster, B., Tait, R., Ooi, C., Bullmore, E. T., & Lutti, A. (2013). Quantitative multi-parameter mapping of R1, PD*, MT, and R2* at 3T: A multi-center validation. *Frontiers in Neuroscience*, *7*, 95. https://doi.org/10.3389/fnins.2013.00095

Williams, O. A., An, Y., Beason-Held, L., Huo, Y., Ferrucci, L., Landman, B. A., & Resnick, S. M. (2019). Vascular burden and APOE ε4 are associated with white matter microstructural decline in cognitively normal older adults. *NeuroImage*, *188*, 572–583. https://doi.org/10.1016/j.neuroimage.2018.12.009

Winklewski, P. J., Sabisz, A., Naumczyk, P., Jodzio, K., Szurowska, E., & Szarmach, A. (2018). Understanding the Physiopathology Behind Axial and Radial Diffusivity Changes—What Do We Know? *Frontiers in Neurology*, *9*. https://doi.org/10.3389/fneur.2018.00092

Ye, Z., Pan, Y., McCoy, R. G., Bi, C., Mo, C., Feng, L., Yu, J., Lu, T., Liu, S., Carson Smith, J., Duan, M., Gao, S., Ma, Y., Chen, C., Mitchell, B. D., Thompson, P. M., Elliot Hong, L., Kochunov, P., Ma, T., & Chen, S. (2024). Contrasting association pattern of plasma low-density lipoprotein with white matter integrity in *APOE4* carriers versus non-carriers. *Neurobiology of Aging*, *143*, 41–52. https://doi.org/10.1016/j.neurobiolaging.2024.08.005

Yeatman, J. D., Wandell, B. A., & Mezer, A. A. (2014). Lifespan maturation and degeneration of human brain white matter. *Nature Communications*, *5*(1), 4932. https://doi.org/10.1038/ncomms5932

Yin, R.-H., Tan, L., Liu, Y., Wang, W.-Y., Wang, H.-F., Jiang, T., Joaquim Radua, Zhang, Y., Gao, J., Canu, E., Migliaccio, R., Filippi, M., Gorno-Tempini, M. L., & Yu, J.-T. (2015). Multimodal Voxel-Based Meta-Analysis of White Matter Abnormalities in Alzheimer's Disease. *Journal of Alzheimer's Disease*, *47*(2), 495–507. https://doi.org/10.3233/JAD-150139

Zhang, H., Schneider, T., Wheeler-Kingshott, C. A., & Alexander, D. C. (2012). NODDI: Practical in vivo neurite orientation dispersion and density imaging of the human brain. *NeuroImage*, *61*(4), 1000–1016. https://doi.org/10.1016/j.neuroimage.2012.03.072

Declaration of Competing Interest

☒ The authors declare that they have no known competing financial interests or personal relationships that could have appeared to influence the work reported in this paper.

Graphical abstract

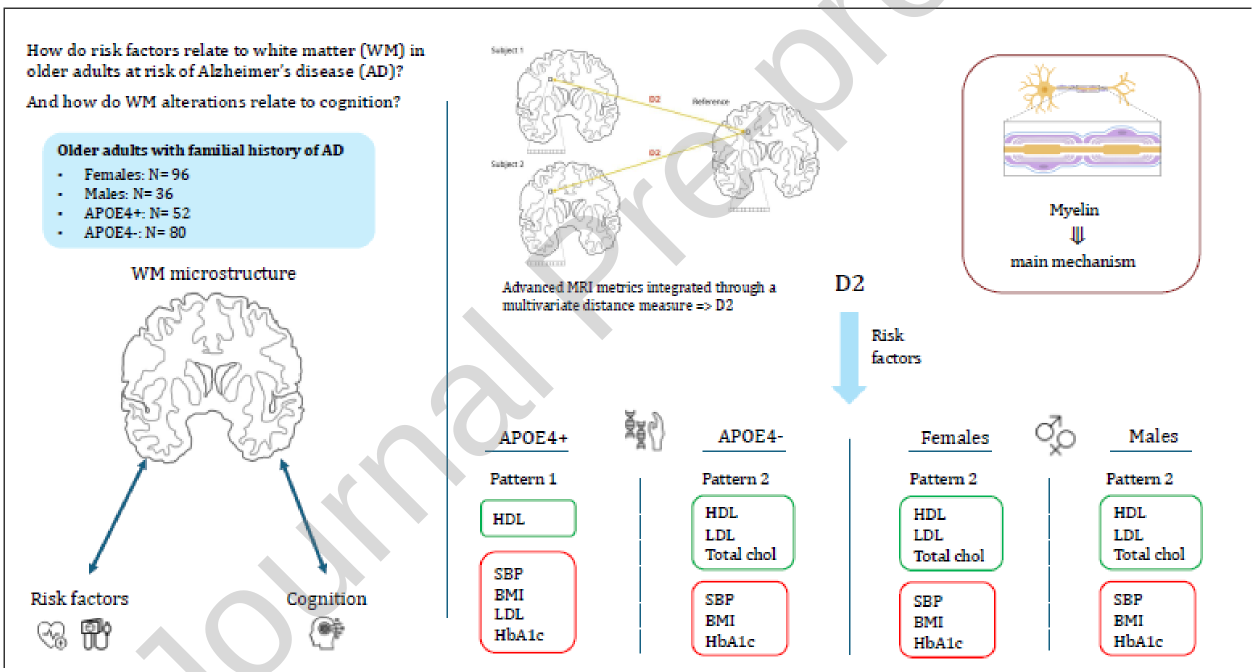

Highlights

- WM alterations were linked to cardiometabolic risk in older adults at risk of AD.
- We identified a distinct risk pattern with LDL-cholesterol in APOE4 carriers.
- WM deviations in APOE4 carriers were linked to immediate memory performance.
- Changes in myelination appeared as the main mechanism underlying WM deviations.